PREPARATION AND CHARACTERIZATION

OF

METAL TITANATE MATERIALS.

BY

PAKAMISA KOBESE

Thesis presented in partial fulfillment for the degree of

Magister Scientiae

at the Faculty of Science at the University of Stellenbosch
Republic of South Africa,

SUPERVISOR: **PROF A. M. CROUCH**

March 2002

"Declaration"

I, the undersigned, hereby declare that the work contained in this thesis is my own original work and that I have not previously in its entirety or in part submitted it at any university for a degree.

Signature:

Date
.....

ABSTRACT

Thin films and powders of Ni_xTiO_3 and Co_xTiO_3 (where x = 0.005 – 0.9) with different stiochiometric ratios were prepared using sol gel techniques. These metal oxides were prepared by spin coating on silicon and titanium substrates followed, by annealing at 400°C and 800°C respectively under a temperature program. A range of films with M_xTiO_y (where x = 0.005 – 0.9) were prepared and then characterized by optical methods such as Scanning Electron Microscopy (SEM), Atomic Force Microscopy (AFM) and Rutherford Backscattering Spectroscopy (RBS). X-ray powder diffraction was also used to determine the structural properties of these metal oxides. XRD pattern peaks showed that the powder forms of these metal oxides were well crystallized. Thin films could be amorphous because strong peaks were not present.

For nickel titanates preparation, the best trend is at the low concentration of Ni that is 0.3:1 Ni:Ti. It is pure with no impurities of NiO and TiO_2. High concentration of Co ranging from 0.7-1:1 Co:Ti forms a Co_2TiO_4 structure with cubic phase. The best route for the $CoTiO_3$ preparation is at the low cobalt concentration that is 0.5:1 Co:Ti.

Scanning Electron Microscopy (SEM) shows that a film deposited on silicon or a titanium substrate is smooth, uniform and crack-free. It also shows that a cobalt titanate film deposited on a Si substrate is rough, with cracks, whereas on the Ti substrate, it is smooth, uniform and crack-free. AFM studies show that as the concentration of Ni:Ti is reduced and the roughness of the thin film is increased. SEM, FTIR, XRD and RBS suggest that the 0.3:1 and 0.5:1Ni:Ti films with 10nm and 11nm thickness, respectively,

have the same structure. RBS suggests that the 1:1 and 0.5:1 Co:Ti have $Co_{1.39}TiO_{2.29}$ and $CoTiO_{4.2}$ structures with 13nm and 16nm respectively. XRD reveals that $NiTiO_3$ and $CoTiO_3$ have rhombohedral crystal structure.

ABSTRAK

Dunlagies en poeiers van Ni_xTiO_3 en Co_xTiO_3 (waar x = 0.005 – 0.9) met verskillende stoigiometriese verhoudings was voorberei deur gebruik te maak van sol gel tegnieke. Hierdie metaal oksiedes was voorberei deur gebruik te maak van "spin coating" op substrate van silikon en titaan gevolg deur konstante verhitting by 'n 400°C en 800°C temperatuur program onderskeidelik. 'n Reeks van lagies met M_xTiO_y (waar x = 0.005 – 0.9) was voorberei en gekarakteriseer met optiese metodes soos Skandeer Elektron Mikroskopie (SEM), Atoom Interaksie Mikroskopie (AFM) en "Rutherford Backscattering Spectroscopy (RBS)." X-straal Poeier Diffraksie was ook gebruik om die strukturele eienskappe van hierdie metaal oksiedes te bepaal. XRD patroon pieke wys dat die poeier vorms van hierdie metaal oksiedes goed gekristalliseer was.

Dunlagies mag ook amorf wees aangesien skerk pieke nie teenwoordig was nie. Vir nikkel titaniete is hierdie die algemene roete vir die $NiTiO_3$ voorbereiding. Die beste tendens is by lae konsentrasies van Ni naamlik 0.3:1 Ni:Ti. Dit is suiwer en het geen onsuiwerhede van NiO en TiO_2 nie. Hoë konsentrasies van Co vanaf 0.7 – 1:1 Co:Ti vorm 'n Co_2TiO_4 struktuur met 'n kubiese fase. Die beste roete vir die $CoTiO_3$ voorbereiding is by lae kobalt konsentrasie naamlik 0.5 – 1:1 Co:Ti.

Skandeer Elektron Mikroskopie (SEM) wys dat 'n $NiTiO_3$ laag gedeponeer op silikon en titaan substrate gelyk was, eenvorming en sonder krake. Dit wys ook dat die kobalt titaan laag oppervlakte gedeponeer op 'n silikon substraat grof was en het krake getoon. Vir die Ti substraat het dit gewys dat die oppervlaktes gladwas, univormig en sonder krake.

AFM studies wys dat as die konsentrasie Ni:Ti verminder word die grofheid van die dunlaag verminder. SEM, FTIR, XRD en RBS dui aan dat die 0.3:1 en 0.5:1 Ni:Ti dunlaag dieselfde struktuur het met 10nm en 11nm dikte onderskeidelik. RBS dui aan dat die 1:1 en 0.5:1 Co:Ti het $Co_{1.39}TiO_{2.29}$ en $CoTiO_{4.2}$ strukture onderskeidelik met 13nm en 16nm diktes. XRD toon aan dat $NiTiO_3$ en $CoTiO_3$ rhombohedrale kristal strukture het.

Dedicated to my Mother and Father

and

I thank the Lord for the strength

ACKNOWLEDGEMENTS

The Author wishes to express his appreciation to:

- Prof A.M Crouch for guidance, encouragement and patience throughout the course of the work.
- Dr C. Theron at NAC, for his help and allowing me to use RBS.
- My colleagues at the Department of Chemistry at U.S.
- Mr D.N Steenkamp in the Department of Physics at U.S for using SEM.
- Sue Malan in Department of Polymer Science at U.S for using AFM.
- Department of Geology at U.S and NAC for using XRD.
- My parents and friends for their unfailing belief in me.
- Dr P Verhoeven in Department of Chemistry at U.S for using FTIR.
- NRF and ESKOM for their financial support.

GLOSSARY OF SYMBOLS

AES = Auger electron spectroscopy

AFM = Atomic force microscopy

CVD = Chemical vapour deposition

NAC = National Accelerated Centre

RAIRS = Reflection-absorption infrared spectroscopy

RBS = Rutherford backscattering spectroscopy

RUMP = Rutherford universal manipulation program

SEM = Scanning electron microscopy

SEXAFS = Surface x-ray absorption fine structure

SIMS = Secondary ion mass spectrometry

STM = Scanning tunnelling microscopy

XPS = X-ray photoelectron spectroscopy

XRD = X-ray diffraction

FTIR = Fourier Transformation Infrared

CONTENTS

LIST OF FIGURES

LIST OF TABLES

CHAPTER 1

METAL OXIDES AND THEIR PROPERTIES

INTRODUCTION AND OBJECTIVES

The metal oxides constitute a diverse and fascinating class of materials whose properties cover the entire range from metals to semiconductors and insulators. Binary oxides contain a metallic element and oxygen, as in TiO_2, Fe_2O_3 or NiO. The range of such compounds is already quite large, but it is greatly extended by considering ternary and even more complex compounds, where additional metallic elements are present (1). These may themselves be transition elements, as in $PbTiO_3$, $SrTiO_3$, $FeTiO_3$, $LaNiO_3$ and etc.

A few transitional metal oxides, such as OsO_4, are volatile compounds consisting of discrete molecules (2). By far the majority, however, are solid under ambient conditions of temperature and pressure. Transition metal oxides may be good insulators, semiconductors, metals (Re_3O) and superconductors ($YBa_2Cu_3O_7$). Many compounds show transitions from metallic to a non-metallic state as a function of temperature (VO_2), pressure (V_2O_3) or composition (Na_xWO_3) (3). Along with these variations in electrical conductivity go wide differences in other physical properties, related to electronic structure.

Metal oxides can occur in nature or can be prepared by various techniques such as sputtering (4), laser ablation (5), reactive co-evaporation (6), sol-gel techniques (7), metal-organic chemical vapour deposition (8) and electrochemical methodologies (9).

The metal oxide surfaces play crucial roles in an extremely wide range of phenomena, for example: the environmental degradation of high-T_c superconductors, bonding

between grains of alumina in sintered ceramics, the passivation of metal surfaces against corrosion, catalysts for the partial oxidation of hydrocarbons, solid-state gas sensors for pollution monitoring and control. The failure of dielectric materials because of surface conductivity and the stability of electrode / electrolyte interfaces in fuel cells, also depend upon the properties of metal-oxide surfaces or the interfaces between metal oxides and other materials (10).

A major milestone in the study of transition metal oxide surfaces occurred in 1972 with the report by Fujishima and Honda that TiO_2 could be used as a catalytic electrode in a photoelectrolysis cell to decompose water into H_2 and O_2, without the application of an external voltage (11). This opened up an area of research in which metal oxides were to be seen as potential catalysts for a variety of reactions. They are also used as sensors for gas reactions.

We therefore embarked on a programme of utilizing metal oxides as potential catalytic surfaces. Metal oxides of the type ABO_3, where A = Ni, Co, B = Ti, will be prepared and characterized. The sol-gel procedure will be used to investigated the preparation of different stoichiometric ratios of the A:B in the ABO_3. The materials will be prepared in powder and thin film form. These materials will be characterized on different substrates. A combination of characterization and bulk characterization tools will be employed to determine the solid state properties of the materials. Thin films will be evaluated for interfacial oxidative processes at the liquid/solid surface.

1.1 METAL OXIDE AND THEIR PROPERTIES

1.1.1 CRYSTAL CHEMISTRY OF PEROVSKITE-PHASE METAL OXIDES

The perovskite structure is known for a range of compounds which include metal oxides, some complex metal halides and a few metal carbides and nitrides (12). The latter three are not included in this introduction. This class of metal oxide, with the empirical formula ABO_3 , is derived from the rare mineral $CaTiO_3$, commonly called perovskite. The structure of this mineral was first thought to be cubic and, although it was later found to be orthorhombic, the name perovskite has been retained for this type. The truly cubic form of this material is referred to as "ideal perovskite" and has a unit cell edge of ~ 4Å, containing one ABO_3 unit. Few perovskite materials have this structure at room temperature, but many assume this structure at higher temperatures (12).

Distortion from the ideal ABO_3 cubic symmetry is common at room temperature and structures with tetragonal, orthorhombic, rhombohedral, monoclinic and triclinic symmetry are known (12). There are many examples of orthorhombic and rhombohedral structures that have been reported, but there are few reports of triclinic, monoclinic and tetragonal systems, although the common phases of these distortions are readily observed by diffraction techniques, where lowering of the symmetry of the unit cell is manifested in the appearance of additional peaks.

The chemical composition of these perovskite-phase materials can vary, depending on the valency of the cations, and includes the following combinations $A^{1+}B^{5+}O_3$,

$A^{2+}B^{4+}O_3$ to $A^{3+}B^{3+}O_3$ (12). In the $A^{1+}B^{5+}O_3$ system, the niobates are the most widely known $KNbO_3$ and $NaNbO_3$ have been studied extensively. Sodium and potassium tantalates are also known to have the perovskite structure (12). Some of the best known perovskite-phase mixed-metal oxide compounds have the formula $A^{2+}B^{4+}O_3$. This is due to the interesting physical properties of certain members of this class, especially $PbTiO_3$ and $BaTiO_3$.

As mentioned above, $CaTiO_3$ has an orthorhombic structure, but $SrTiO_3$ is truly cubic while the atomic displacements from idealized lattice sites in $PbTiO_3$ and $BaTiO_3$ result in their ferroelectic properties. Both $PbTiO_3$ and $BaTiO_3$ become cubic at higher temperatures; $PbTiO_3$ changes from tetragonal to cubic at 490^0C while $BaTiO_3$ undergoes three transformations: rhombohedral to orthorhombic at -90^0C, orthorhombic to tetragonal at 0^0C, and tetragonal to cubic at 130^0C. The last group of oxides with the formula $A^{3+}B^{3+}O_3$ is usually found for the rare earth derivatives. None of these compounds have the ideal perovskite structure, but some of the rhombohedral perovskites are only slightly distorted from the ideal cubic perovskite structures.

1.2 PROPERTIES OF PEROVSKITE-PHASE MATERIALS

Perovskite-phase metal oxides exhibit a variety of interesting physical properties which include ferro-electric, dielectric, pyroelectric and piezoelectric behaviour. Dielectric materials are electrical insulators (the response of a conducting material to a low-frequency electric field is dominated by the mobile charge carries) for which the response to a weak static or low-frequency electric field is given by

$$P=\varepsilon_o \chi E$$

where P is the electric polarization (dipole moment per unit volume), E is conventionally the macroscopic electric field inside the material, ε_o is the permittivity of free space and χ is the electric susceptibility(13). Pyroelectric materials possess an electric polarization in the absence of an applied electric field. Each primitive unit cell has a dipole moment associated with it. The prefix pyro- comes from the Greek word for fire and is used in this context because a macroscopic dipole moment is only seen when the material is heated; the dipole moment is normally neutralized by ions and electrons that collect on the surface of the sample (13).

Ferroelectric materials are pyroelectric only below a certain temperature, which is characteristic of the material. They are so called because they are the electric analogues of ferromagnets, not because they are associated with iron. Ferroelectric transitions can arise in a number of different ways. One possibility occurs in molecular solids containing polar molecules that are able to rotate at high temperatures; if rotation ceases on cooling, the dipole moments can align to give a spontaneous electric polarization (13).

In piezoelectric materials the polarization is changed by applying a stress as well as by changing the electric field; for small stresses the polarization depends linearly on the stress. All ferroelectric materials are piezoelectric but the converse is not true; quartz is the best known example of a material that is piezoelectric but not ferroelectric. Piezoelectric materials are widely used as transducers for the interconversion of electrical and mechanical energy. Important applications include the generation and

detection of ultrasonic waves, the electrical control of small displacements (in optical systems and in the scanning tunneling microscopy for example) and surface acoustic wave (SAW) devices (13).

These properties are defined as follows (14-18). Linear dielectric materials exhibit linear polarization behaviour as a function of applied field. Ferroelectric ceramics are a group of electronic materials consisting of dielectrics with a permanent electric dipole which can be oriented by the application of an electric field. Pyroelectric materials exhibit a spontaneous polarization, but the direction of the polarization cannot be reversed on application of an electric field. Piezoelectric materials exhibit an electric charge when mechanically stressed, or undergo mechanical deformation on the application of the electric field. These properties arise from the crystal symmetry adopted by these materials and its relationship to the symmetry of its physical properties. The equilibrium properties of a material can be described in tensor notation and be transformed by symmetry operations. Neumann's principle states that the symmetry elements of any physical property of a crystalline material must include all the symmetry elements of the point group of the crystal.

The physical properties may, and often do, possess more symmetry elements than the point group. As a result it is possible to predict the physical properties of a crystalline material based on crystal symmetry. The seven crystal systems (cubic, hexagonal, trigonal, tetragonal, orthorhombic, monoclinic and triclinic) are comprised of 32 crystal classes according to their point group symmetry. Of the 32 classes, 20 are piezoelectric and 10 of these (1, 2, m, 2m, 2mm ,4, 4mm, 3, 3m, 6, and 6mm or C_1, C_2, C_{1h}, C_{2v}, C_4,

C_{4v}, C_3, C_{3v}, C_6 and C_{6v}, respectively in the Schoenflies notation) possess spontaneous electrical polarization and are termed " polar". The polar axis of the crystal is a direction that is parallel to the spontaneous polarization vector. The internal or external electrical conduction generally cannot provide enough current to compensate for the charge in polarization with temperature in a polar crystal. As a result, the crystal develops an electric charge on its surface and therefore polar crystals are pyroelectric.

Ferroelectric materials are a subgroup of polar materials and they are therefore both pyroelectric and piezoelectric (14,19). Ferroelectric materials are currently a great deal of interest because their electric dipole can be reoriented by the application of an electric field. However, all of these materials lose their polar properties above the Curie temperature, T_C, and the nonpolar state above this temperature is called the paraelectric phase. For example, barium titanate changes from the tetragonal ferroelectric phase to the paraelectric cubic phase at 130^0C, the Curie temperature.The properties of ferroelectric materials change significantly and show a maximum as the temperature approaches T_C. In the case of $BaTiO_3$, the dielectric constant increases from 1000 to ~ 10 000 in the 10K interval below the T_C, while above this temperature there is a gradual decrease in the dielectric constant. The main applications for $BaTiO_3$ are based on this phase transition, especially applications as a dielectric. The temperature at which these phase transitions occur can be modified by the partial substitution of other metal oxides into $BaTiO_3$, to give solid solutions (20). These substitutions by dopants change the cell dimensions and hence the temperatures at which the phase changes occur. Not all perovskite- phase metal oxides of this type exhibit ferroelectric properties. For example, $CaTiO_3$ and $SrTiO_3$ exhibit simple linear

dielectric behaviour; they possess high dielectric strength and have low dielectric loss.

1.3 PROPERTIES OF METAL OXIDES

Metal oxides have certain properties, namely: electronic, ionic, interfacial, and electrochemical properties.

(a) Electronic properties.

A general condition for the semiconducting behaviour of transition metal oxides is that the metal ion should be capable of existing in several valence states, so that conduction can take place by electron transfer from low to high valence states. A strong electron-photon coupling is usually observed in transition metal oxides leading to the formation of a so called "small polaron" (21). The strong interaction between the unpaired electron and polar oxide network leads to the polarization of the lattice and a displacement of oxygen ions around the low valence transition metal ion. When these distortions are limited to the nearest neighbours, the unpaired electron becomes trapped in its potential well (22). A "small polaron" is formed, characterized by its binding energy, that is usually about 0.5eV for most transition metal oxides (23). Small polaron hopping between two neighbouring sites occurs when both sites have the same potential energy. This is achieved by lattice distortions and phonons must be involved in the hopping process. The hopping rate, however depends on two factors:

I. a phonon term corresponding to the probability for both sites to have the same potential energy.

II. an electronic term corresponding to the probability for the electron to tunnel from one site to the other.

(b) Ionic properties

From a chemical stand point, transitional metal oxides are hydrous oxides. They correspond to the general formula $MO_x.nH_2O$ and can be defined as " particle hydrates" according to the classification suggested by W.A. England et al (24). The particle hydrates consist of charged particles separated by an aqueous solution. The structure within a particle is that of the anhydrous oxide and the particles are linked together to form agglomerates. The full co-ordination at the surface of the particle is preserved by water molecules. Additional water molecules occupy the inter-particle region to produce a connected, viscous liquid region through the composite solid. A protonation equilibrium exists at the oxide-water interface. This makes the liquid –like region acidic or basic, depending on the nature of the oxide network. Acidic dissociation occurs by large metal atoms of low charge (25). Thus particle hydrates exhibit some common features such as good ion exchange properties or fast proton conduction.

(a) Electrochemical properties

Electrochromic display devices and electrochromic layers based on amorphous WO_3 thin films have been extensively studied (26). Such films can exhibit two stable states, one which is transparent while the other one is blue. Reversible coloration and bleaching can be easily obtained in an electrochemical cell. Other transitional metal oxides also exhibit electrochromic properties and can be deposited via the sol-gel process. TiO_2 films have been made from titanium tetrabutoxide. They reversibly turn from white to blue (26). V_2O_5films deposited from a polyvanadic acid sol turn from yellow to green upon cation of a voltage of $\pm$ 1.5 (27).

(b) Interfacial properties

When a metal oxide (semiconductor) is brought into contact with an aqueous solution, an electron transfer process occurs at the oxide-water interface until the electrochemical potentials of both become equal. As a result of this transfer, the oxide surface becomes charged with respect to the solution. The charge is actually distributed over a region, the thickness of which depends on the doping level of the semiconductor. For a weakly doped oxide, the space charge layer is typically more than $100A^0$ (28).

In this project we concentrate on the manufacture and photocatalystic properties of certain metal oxides such as $NiTiO_3$ and $CoTiO_3$, that are prepared by sol-gel techniques.

1.2 SOL-GEL TECHNIQUES

1.2.1 INTRODUCTION

The sol-gel process has recently increasing interest because it permits the development of new shapes (fibers, thin films and near net shape objects) with good homogeneity and good purity. The the sol-gel method was first used in 1845 by M. Ebelman who obtained the formation of solid, glassy silica upon the slow reaction of tetraethyl orthosilicate with moisture (29). It was, however, more than a century later that researchers began using the sol-gel technique as a method of synthesis. Interest in the use of this technique has grown to such an extent that hundreds of scientific papers on the sol-gel technique are new published each year.

To understand the concept of sol-gel, it is important to understand the difference between sols and gels:

Sol is a dispersion of solid particles in a liquid phase where the particles are small enough to remain suspended indefinitely by Brownian motion. For aqueous sols this means a particle size of less than approximately 1 micron (29). Electrostatically stabilized sols can contain far higher equivalent oxide concentrations than the solubility limits of the solutions from which they are derived (30).

Gel is a solid containing a liquid component and an internal three dimension network structure so that both the solid and the liquid are in a highly dispersed state (29,30). Not all sols can be converted to gels. An important criterion for gel formation is that

there must be a strong particle solvent interaction so that at least part of the solvent is bound. However, sols are thermodynamically unstable as a result of the relatively high surface to volume ratio, which increases the Gibb's energy at the surface. This fact increases the chance of flocculation and coagulation (30).

The sol-gel method has gained its popularity because of its many advantages. These can be summarized as follows

1. Better homogeneity from raw materials is obtained
2. Better purity from raw materials is obtained
3. Lower temperature of preparation, impliying that:
   (a) Energy is saved
   (b) Evaporation losses are minimized
   (c) Minimized air pollution
   (d) No reaction with containers, thus purity
   (e) Phase separation
   (f) Crystallization
4. New non-crystalline solids outside the range of normal glass formation
5. New crystalline phases from crystalline solids
6. Better glass products
7. The creation of special products such as films

Despite these advantages, the sol-gel process does have its drawbacks too, namely:

1. The price of technology for products, such as plasma-spray powder and catalyst, is very high. The sol-gel process is normally not economically suitable for the productions of large quantities of a product, thus even in future it will not replace any "heavy" industrial procedure (31).

2. The size of ceramic objects produced by the sol-gel process is limited as a result of the necessity of extracting the liquid phase (32).

1.1.2 METHOD

The synthesis of oxide materials the sol-gel process can be described as the progressive formation of a solid network as a result of an inorganic polymerization reaction. This series of reactions can be summarized as comprising five main parts.

1. The components are mixed on an atomic scale and an "ultra homogeneous" product is obtained.
2. The activities of some species (such as H^+; OH^- and other ions) are adjusted so as to form a sol.
3. Gelation is controlled principally by pH, ionic strength, temperature and time, and these parameters need to be established for each individual synthesis.
4. The gel is shaped to the desired form use.
5. Drying and heat treatment leads to the formation of the product at a lower temperature and in a shorter time than required in other methods (32).

There are two different routes which can be used, depending on the nature of molecular precursor: the inorganic route, with metal salts in aqueous solutions, and the metal-organic route with metal alkoxides in organic solvents (29,33). For the aqueous-based process, the formation of the sol is accomplished by the hydrolysis of the metal cations:

$$M^{n+} + nH_2O \longrightarrow M(OH)_n + nH^+$$

The addition of a suitable base pushes the reaction to the right, causing the precipitation of finely divided hydroxide, which is then peptized by the addition of the mineral acid. This causes protons to be absorbed onto the particle surfaces to generate a net positive surface charge, which is balanced by the anions from the acid.

Electrostatic attractions and repulsion inhibit inter-particle contact, thus a stable sol is produced. Another method of stabilizing a sol is to add a dilute solution of a long chain polymer to the precipitate. The long-chain polymer contains active chemical groups which are receptive to the hydroxyl groups on the surface of the precipitate. They are thus adsorbed onto the particle surfaces and become sterically stabilized. Interactions are hindered by the long-chain molecules extending out from the surface (30). The gelation process for the aqueous-based method is accomplished either by the removal of water (dehydration gelation), or an increase in the pH (alkaline gelation). The restraining energy barrier is thus removed and the sol spontaneously coagulates to form a gel. The alcohol-based process involves reactions with metal alkoxides where nucleophilic substitution of the alkoxy ligands by a hydroxylated species (TOH) occurs:

$$M(OR)_z + nTOH \longrightarrow M(OR)_{z-n}(OT)_n + nROH$$

where T can be H (i.e., hydrolysis occurs), a metal atom (condensation) or an organic/ inorganic ligand (complexation) (57). The overall reaction is given by:

$$M(OR)_4 + 2H_2O \longrightarrow MO_2 + 4HOR$$

There is no distinct sol formation step, but rather simultaneous hydrolysis and

condensation reactions which eventually yield the gel. Hydrolysis in a neutral environment requires a longer reaction time to achieve the required extent of the reaction. This implies that hydrolysis must be catalyzed by the addition of an acid or a base and excess of water is most often used for the hydrolysis. The properties of the gel are sensitive to parameters such as the water to alkoxide ratio, temperature, solvent and the nature of the catalyst (30), since partial hydrolysis leads to greater polycondensation and thus affects the texture of the gel. Monoliths, coatings and fibres are generally obtained from acid environments whereas powders are formed in a basic environment (33). A further effect of pH, which was observed in the synthesis of lead titanate, is that acidic gels are more capable of polymeric rearrangement during drying, yielding a denser, amorphous structure with micro-crystalline regions (34).

Most preparation methods involve the use of titanium tetra-alkoxide dissolved in dry alcohol such as isopropanol or methoxyethanol. Metal salts such as $Sr(OH)_2$ and $Ba(OH)_2$ were also dissolved in dry alcohol and the two solutions were mixed together and the gel was formed (35,36). It was generally found that the main problem with the use of a titanium alkoxide was susceptable to hydrolysis by even traces of moisture and rapid condensation reactions occurring between Ti-OH groups in basic media. This involves the growth of polymeric species that contained either -OH or -O- bridges forming a highly cross-linked Ti-O network. It was noticed that ease of hydrolysis decreased with increasing chain length of the alkyl group (37,38). This problem led Rehspringer et al (39) to conduct experiments in an inert gas flow and sheltered from moisture to prevent premature precipitation. They also decided to carry out lower temperature reactions inorder to control the hydrolysis kinetics, as they found the water sensitivity of alkoxides precluded the use of acids or bases for the

polycondensation reactions. Their use of inert gas flow was the successful experiment that lead to the formation of a yellow gel.

Once the gel was formed, it needed to be deposited on substrates to form thin films.this was to be followed by heat treatment (annealing or calcination) in order to remove the organic ligands, or the gel could be dried before heat treatment (calcined) to form powders.

1.3 SURFACE SCIENCE TECHNIQUES

1.3.1 INTRODUCTION

Why surfaces?

The growth in the study of solid surfaces and in the number of techniques available for their study has been enormous since the early 1960s. At least one reason for this is the growing awareness of the importance of understanding surface properties and the fact that work on surfaces has had an impact on this understanding and on specific applications in the 'real world'. At a fundamental level surfaces are of great interest because they represent a rather special kind of defect in the solid state. Much of our understanding of solids is based on the fact that they are, in essence, perfectly periodic in three dimensions; the electronic and vibrational properties can be described in great detail using methods which rely on this periodicity. The introduction of a surface breaks this periodicity in one direction of localized electronic and vibrational states.

Gaining a proper understanding of these effects is not only of academic interest, as there is growing interest in the properties of low-dimensional structures in semiconductor devices, and a free surface can represent the simplest case of such a structure. The commercial availability of ultra-high vacuum in the 1960s prompted enormous academic interest in the science of surfaces and interfaces. A number of the techniques used initially for basic studies have since been developed into sophicated and widely used methods for routine surface analysis. Viable new techniques are still being invented and the established methods are still being improved at a pace. These techniques are electron and ion spectroscopies, methods for surface structure determination, as well as the atom-imaging methods.

1.3.2 SURFACE STRUCTURE DETERMINATION

The behaviour of the outer surface atomic layer and its interaction with atoms or molecules of adsorbates is the cornerstone of surface science. A complete understanding, at the atomic level, of these basic interactions would have important technological spin-off since they are crucial to all surface chemical reaction, catalysis and thin film nucleation. The adsorbed species can include organic and biological species. A synchroton radiation source is required to provide an intense beam of X-ray, although recent developments using electron sources affect the technique because it does not require long range order (40). Infra-red spectroscopy to study the vibrational spectroscopy to give bonding geometries and orientation information. FTIR has a unique ability to characterize surfaces in the presence of high ambient pressures of gases simulating reaction conditions typical in industrial catalysis. The technique has provided valuable information on the interaction of hydrocarbon, particularly on metal surfaces.

1.3.3 THE ION SPECTROSCOPIES

In general terms, the ion spectroscopies involve bombarding a surface with ions or energetic neutrals and measuring the mass or the energy of the emitted species. Their development has lagged behind those of the electron spectroscopies, but it is now the area where progress is most rapid. Secondary Ion Mass spectroscopy (SIMS) is probably the most popular of the ion based techniques. In SIMS, a beam of ions (or neutrals) is used to remove surfaces atoms, the ionized fraction of which is analyzed in a mass spectrometer (41). Recently, exciting developments have been made in Medium Energy Ion Scattering (MEIS). These have been aimed to overcoming the problem of

surfaces neutralization. In principle, MEIS is a highly sensitive , quantitative technique with a cost and size that will make it highly attractive as a surface analysis tool. In many ways, MEIS could become the laboratory equivalent of Rutherford ackscattering spectroscopy (RBS) and its allied techniques. In RBS, a MeV beam of light ions is used as a primary ion source. Measurements of the scattered particles lead to a fully quantitative composition and depth analysis without the need for reference standards. RBS is a mature technique and easily the most quantitative (±5% accuracy).

1.3.4 THE ELECTRON SPECTROSCOPIES

Both X-ray photoelectron spectroscopy (XPS) and Auger electron Spectroscopy (AES) have been available commercially for about 25 years and have both progressed to advanced stages of development. Two techniques have been incorporated into a multitechnique instrument. In XPS, the sample is illuminated with X-rays, which excite photoelectrons from the sample surface. The photoelectron energy is dependent on the chemical environment and pronounced chemical shifts are produced in the position of the peaks in the energy spectrum and hence a major advantage of XPS is its ability to provide chemical state information.

Since X-rays do not normally cause radiation damage, the technique is amenable to a wide range of sample materials including polymers, organic coatings and insulating powder materials (42). In AES a beam of electrons is used to excite Auger electrons from the surface. By using an electrostatically focused beam, Scanning Electron Microscopy (SEM) techniques can be used to obtain both a secondary electron image as well as an elemental image of the region under analysis. In many ways, SEM and dedicated AES instrumentation techniques are merging with useful spartial resolution

using field emission electron sources of 50nm. Small and well-defined area analysis also lends itself to composition depth profiling. This is a particular strength of AES and SEM is applied way to the characterization of a vast range of thin films, multilayer stacks and surface coatings.

1.3.5 THE ATOM IMAGING TECHNIQUE

The development of the Scanning Tunneling Microscope (STM) and its close cousin the Atomic Force Microscope (AFM) over the last decade has been remarkable. A highly competitive variety of instruments are now commercially available to cover applications in air and under ultra-high vacuum where atomic resolution is possible. It has become a powerful means of local surface topography measurement. Useful variants such as the magnetic force microscope provide valuable data on magnetic domain structures and there is also the prospect of using electron spin resonance techniques to provide composition information.

In this project, certain surface techniques are used to characterize the thin metal oxide films. These are chosen by their extent to provide powerful information to characterize thin surfaces. The SEM and AFM are used to study the surface morphology of the thin films. RBS for cation stoichiometry and thickness of surfaces and X-ray powder diffraction to determine the crystal structure of materials. FTIR to check organic residues on the surface.

1.4 CHARACTERISATION TECHNIQUES.

1.4.1 X-RAY DIFFRACTION

X-rays are forms of electromagnetic radiation that have much shorter wavelength, and thus much higher energy than visible light. X-rays can be formed in a number of different ways, but the method most used in x-ray diffraction experiments is to have accelerated electrons strike a target anode, thus emitting x-rays with a wavelength characteristic of the anode material.

All materials interact with electromagnetic radiation to a greater or lesser extent. Amorphous solids absorb, transmit or scatter the radiation in all directions, whereas crystals as a result of their ordered arrangement interact with radiation in a more ordered manner. If the wavelength of the electromagnetic radiation is of the order of the pattern repeat distances, as in the case of x-rays, then diffraction becomes important. As a result of the ordered nature of a crystal this leads to constructive and destructive interference of the scattered beams of x-rays that in turn results in diffraction patterns that can be interpreted to give information about the structure being studied.

In 1912 Laue et. al.(43) proved experimentally that it was possible to diffract x-rays by means of crystals, yet it was only later that the full impact of this discovery was realized when Bragg reported the important conditions for diffraction in a simple mathematical form, that is known as Bragg's law. They were also able to determine crystal structures of NaCl, KCl, KBr, and KI. They achieved this success by viewing

the periodic arrangement of crystals as consisting of layers of planes parallel to each other at a distance d from each other.

In general, radiation scattered by adjacent electrons is not in phase. Only when it is, will reinforcement occur and a diffracted beam can be observed. Bragg determined that this constructive interference only occurs if the differences in the distances travelled by the waves reflected from successive layers is a whole number of wavelengths, i.e. as expressed by Bragg's law:

$2d\sin\theta=n\lambda$

Where d = interplanar spacing

λ = wavelength

n = integer (1,2,...)

The requirement that n may only be a whole number means that a reflection will be observed at specific angles (i.e. specific values of θ). The planes are labelled using sets of integers called crystal indices. A set of planes, whose indices are h, k, and l, intercept the x, y, and z-axis. When a single crystal is irradiated with x-rays, the incident x-ray beam passes through a hole in a photographic plate and the diffracted beams are detected as spots on the developed film. The positions of these spots are governed by the arrangement of the atoms within the crystal structure. However, not all the diffracted beams will have the same intensity, as the intensity of a diffracted wave depends on the electron distribution of the crystal since x-rays are scattered by electrons. Thus increasing numbers of electrons will lead to diffracted beams with increasing intensities. This is not always true however, as symmetries within the crystal can lead to some diffracted beams being extinguished known as systematic absences.

In a crystal structure determination, a partial data collection is first made to determine the size and shape of the unit cell. From the intensity of the different spots, systematic absences are observed which give an indication as to what crystal belongs to. The number of atoms per unit cell can be calculated from the size and shape of the unit cell, chemical composition of the compound and its measured density. Thereafter, a complete data set is collected and the indices can be assigned to each diffraction beam, known as the indexing pattern. The data is then calculated through various procedures to give the positions of the atoms.

In powder diffraction, an incident beam of x-rays interacts with a specimen that is in the form of either a small non-diffracting filament containing bonded powder or a polycrystalline fibre of very small grain size. The specimens must contain sufficient particles with the correct orientation to allow diffraction from all possible diffracting planes when rotated in the x-ray beam 2θ and consequently each set of crystal planes produce x-rays of semi-angle 2θ. A film placed around the specimen intersects the different conics and produces curves concentric with the entrance and exit apertures. The position of intensity peaks in the diffracted beam is characteristic of the material being examined and known phases may be identified by comparison to standards. These are found in the Powder Diffraction File which is a collection of all the known powder diffraction patterns(almost 60000 pattern), containing a list of peak-intensities (that is expressed as a percentage of the most intense peak) versus d-spacings (that are calculated from Bragg's law). The d-spacings are used as opposed to the 2θ values, as they are independent of the wavelength of the radiation used for data collection. For a sample containing a mixture of phases the diffraction pattern collected will be a

combination of the diffraction patterns of each of the phases, that allows for the identification of all the individual phases. X-ray diffraction is thus a technique that can be used for the identification of a crystalline sample, crystal structure determination and analysis of a polycrystalline mixture of phases (both qualitative and quantitative).

1.4.2 RUTHERFORD BACKSCATTERING SPECTROSCOPY (RBS)

INTRODUCTION

Ion Scattering spectroscopy which has been reviewed by Mackintosh is concerned with elastic scattering of ions from surface atoms (43). As the energy of the incident ion beam increases the ions penetrate into the material and in doing so they will lose energy due to inelastic collisions. In this case the ions may be elastically scattered from the surface while the ions that have lost energy may be elastically scattered by atoms in the bulk. By measuring the energy and intensity of the backscattered ions it is possible to identify the position and concentration of the impurity atoms. The technique is known as Rutherford Backscattering (RBS).

Theory

The energy ,E_1 of an ion of mass M_1 scattered by a surface atom of mass M_2 in a direction θ to the incident ion that has energy E_0 is given by

$$E_1 = C^2 E_0 \ldots\ldots \qquad (1)$$

Where $$C = \frac{M_1 Cos\theta}{M_1 + M_2} + \left\{ \left(\frac{M_1 Cos\theta}{M_1 + M_2} \right)^2 + \left(\frac{M_2 - M_1}{M_1 + M_2} \right)^2 \right\}^{1/2} \ldots\ldots\ldots(2)$$

Ions which have penetrated below the surface will lose energy (E_0 - ΔE_0) and the elastically scattered ions will also lose energy (E_1 –ΔE_1) in reaching the surface. The rate of energy loss is given by the stopping power S_p and the energy E_1^* emerging from the surface following scattering at a depth X below the surface is given by

$$E_1^2 = \left(E_0 - \int_0^{i=x\sec\theta_1} S_p(E)dr \right) C^2 - \int_{i=x\sec\theta_2}^{0} S_p(E)dr \ldots\ldots\ldots\ldots \qquad (3)$$

Where r_1 and r_2 are the distances of the incoming and outgoing particle trajectories,

and θ_1 and θ_2 are ingoing and outgoing particles angle directions. The number of particles scattered is directly related to the number of particles in the specimen material, thus by measuring the flux of backscattered ions the concentration of that element in the target can be determined. To a first approximation the ratio of the number of counts in an impurity peak, I_i to the number in one channel of the substrate I_s, is given by

$$\frac{I_i}{I_s} = \frac{Z_i^2 N_i}{Z_s^2 N_s} \frac{E_0^2}{\left(E_0 - \int_0^{x \sec\theta_1} S_P(E) dr\right)^2} \quad \text{.....(4)}$$

Where Z_i and Z_s are the atomic numbers of the incident and target atoms respectively, is the number of impurity atoms and N_s is the number of substrate atoms contributing to the selected channel and the other terms are as defined above. The stopping power S_p can be determined from look-up tables that have been produced for most ions and energies.

1.4.3 SCANNING ELECTRON MICROSCOPY

INTRODUCTION

During the last couples of decades, Scanning Electron Microscopy (SEM) has become an important scientific tool throughout the broad range of applied and basic research endeavours. Its utilization extends from the world of the physicist and the engineer to the biologist, with many users throughout the scieces.. The outstanding contribution of the SEM to science has resulted in part from the instrument's ability to combine high magnification with great depth of field (44). The SEM can also produce images over a wide range of magnifications, thus bridging the magnification gap between light microscopy and the transmission electron microscope. Additionally, the variety of electron induced signals which are produced in the SEM can yield a great deal of morphological, physical and chemical information about a specimen (45).

Instrumentation

The electron gun operates typically over a voltage range 0 to 30 KeV, sometimes extending up to 60 keV, depending upon the type of instrument and application where the specimen is maintained at earth potential. The microscope is a probe forming system where each lens condenses and demagnifies the electron to a focused spot at the specimen surfaces. Electron probes of sizes down to ~6 nm can be achieved with conventional thermionic emission source although smaller probes ~1.5 nm require higher intensity or 3.5nm at low intensity (100kV) using coherent field emission sources. The electron is scanned by the incident electron and electrons emitted from the surface are collected and amplified to form a video signal.

1.4.4 ATOMIC FORCE MICROSCOPY (AFM)

INTRODUCTION

The Atomic Force Microscope (AFM) is being used to solve processing and materials problems in a wide range of technologies affecting the electronics, telecommunications, biological, chemical, automotive, aerospace, and energy industries. The materials being investigating include thin and thick film coatings, ceramics, composites, glasses, synthetic and biological membranes, metals, polymers, and semiconductors. The AFM is being applied to studies of phenomena such as abrasion, adhesion, cleaning, corrosion, etching, friction, lubrication, plating, and polishing. By using AFM one can not only image the surface in atomic resolution but also measure the force at nano-newton scale.

The publications related to the AFM are growing speedily since its birth. The first AFM was made by meticulously gluing a tiny shard of diamond onto one end of a tiny strip of gold foil. In the fall of 1985 Gerd Binnig and Christopher Gerber used the cantilever to examine insulating surfaces. A small hook at the end of the cantilever was pressed against the surface while the sample was scanned beneath the tip. The force between tip and sample was measured by tracking the deflection of the cantilever. This was done by monitoring the tunneling current for a second tip positioned above the cantilever. They could delineate lateral features as small as 300 Å. The force microscope emerged in this way. In fact, without the breakthrough in tip manufacture, the AFM probably would have remained a curiosity in many research groups. It was Albrecht, a fresh graduate student, who fabricated the first silicon microcantilever and measured the atomic structure of boron nitride. Today the tip-cantilever assembly

typically is microfabricated from Si or Si_3N_4. The era of AFM came finally when the urich group released the image of a silicon 7X7 pattern. The world of surface science knew that a new tool for surface microscope was at hand. After several years the microcantilevers have been perfected, and the instrument has been embraced by scientists and technologists.

Operation

An atomically sharp tip is scanned over a surface with feedback mechanisms that enable the piezo-electric scanners to maintain the tip at a constant force (to obtain height information), or height (to obtain force information) above the sample surface. Tips are typically made from Si_3N_4 or Si, and extended down from the end of a cantilever. The nanoscope AFM head employs an optical detection system in which the tip is attached to the underside of a reflective cantilever. A diode laser is focused onto the back of a reflective cantilever. As the tip scans the surface of the sample, moving up and down with the contour of the surface, the laser beam is deflected off the attached cantilever into a dual element photodiode. The photodetector measures the difference in light intensities between the upper and lower photodetectors, and then converts to voltage. Feedback from the photodiode difference signal, through software control from the computer, enables the tip to maintain either a constant force or constant height above the sample.

1.4.5 FT-IR spectroscopy

Introduction

Infrared spectroscopy was among the first techniques to be applied to the direct characterisation of adsorbates, with the earliest investigations of adsorption on finely divided materials (46). These early studies employed transmission infrared spectroscopy, in which the infrared beam passes through a suitably prepared sample and the change in its absorption spectrum following adsorption is monitored. Applications of this technique to studies of heterogeneous catalysis soon followed and a considerable body of literature had been amassed by the end of the 1960s. Subsequent instrumental developments, notably including the increasing availability of Fourier Transform Infrared (FT-IR) spectrometers, advanced the technique.

While transmission infrared spectroscopy still constitutes the principal means of studying catalyst surfaces directly, there is an evident advantage in extending infrared techniques to the study of single crystal samples that can be characterized by other surface probes such as various electron spectroscopes. Reflection-absorption infrared spectroscopy (RAIRS), one technique that enables this to be done, was first applied many years ago.

Although FT-IR was used in one of the earliest applications of RAIRS, the instrumentation required did not become generally available until the 1980s, so that the vast majority of studies performed prior to 1985 utilised dispersive spectrometers (47). Attaining sufficient sensitivity proved to be a major problem with these instruments, and a variety of techniques were developed to achieve this, including polarisation

modulation, wavelength modulation and infrared ellipsometry (48). However, following the publication of the first FT-RAIRS spectra obtained under ultrahigh vacuum conditions, it became apparent that FT-IR could achieve high surface sensitivity without recourse to such specialised methods and most workers now use FT-IR spectrometers.

Instrumentation

In the analysis of organic compounds, the infrared spectrum gives the most information about the compounds structures. A molecule is constantly vibrating, i.e. bonds stretching and bending with respect to each other. Changes in the vibration of molecules are cause by absorption of infrared light. In FTIR the sample is placed in the infrared light in such a way that the infrared beams can be absorbed by the sample. The infrared spectrum of absorbance versus wavelength will be plotted that reveals the presence or absence of characteristic groups within their fingerprint region because of their characteristic absorption bands.

Application

FT-IR is a widely used industrial tool for the structural and compositional analysis of organic, inorganic, or polymeric samples and for quality control of raw materials and commercial products. The infrared absorption of inorganic substances can also be performed but their absorption bands are found at frequencies below 400 cm^{-1}, e.g. $BaTiO_3$ at 610 - 495 cm^{-1} and $SrTiO_3$ at 610 cm^{-1} and 395 cm^{-1} (49).

1.5 THIN FILMS

1.5.1 INTRODUCTION

A very considerable part of our industry is involved with thin films. Much of this is well established, as in the use of electroplated films for protection or decoration. Much of it is of recent origin and involves the use of techniques which have been developed over the last few years. In one way and another most physical properties of films- optical, chemical, magnetic, electrical, etc.- are of importance in an ever widening sphere of industrial, scientific and technical applications. At the same time studies of the fundamentals of film formation and of the basic reasons for differences in behaviour between films and bulk materials are being pursued with increasing vigour. With the development of sophisticated methods of production and examination, our understanding of many of the apparent vagaries of film behaviour is steadily improving. Many of the discrepancies in our early experiments on films are now known to have arisen from factors whose influence was unknown or unsuspected. Advances in many of the necessary accompanying technologies have enabled work on films to be carried out under conditions admitting a high degree of control.

1.5.2 METHODS OF PREPARATION OF FILMS

The methods commonly used to prepare thin films of solid may be classified under the following headings:

i. Electrolytic deposition, which includes cathodic and anodic deposition;

ii. Sputtering, including the more recently developed method of reactive sputtering;

iii. Deposition in vacuum from a heated source (thermal evaporation);

iv. Deposition from vapour reactants;

v. Diffusion.

In some cases, method (iii) may be used reactively, by introducing a gas which reacts with the evaporated material. The main characteristics of these methods are given below.

(I,a) Electrolytic deposition – cathodic films

The method of making metal coatings by electrolytic deposition on the cathode of a cell is probably one of the oldest known methods for making films artificially. Superficially, the method is simple. Ions in the solution are impelled to the electrodes by the applied electric field. At the electrodes, the charges are neutralized and straight deposition may occur. Alternatively reactions may occur between the resultant atoms or radicals and the electrode or bath materials.

The laws governing the overall process are well-known but factors governing the precise form and microstructure of films formed in this way are less well understood. A simplified view of the electrolytic deposition process, inadequate in detail but giving an indication of the main factors influencing the process, may be seen as follows. A double layer forms at the cathode of the system, formed by the electrons in the metal and the ions adsorbed on the surface. In this region, the dominant forces are of short range. Adjacent to this region is a diffusion layer, lying between the cathode and the main body of the electrolyte. In the latter, the electrolyte concentration is substantially constant and the transport of ions is effected by the applied electric field. In the cathode diffusion layer, the combined effects of the ions is governed both by diffusion and by electrical forces.

(I,b) Electrolytic deposition – anodic films

When certain metals are made the anodes of electrolytic cells, oxide film formation occurs, leading frequently to extremely hard, compact well-adhering coatings. Anodized aluminium articles have long been generally available – excellent examples of the way in which the normally highly reactive aluminium is completely protected by the anode film. The electrolytic capacitor forms another everyday example of the use of such films. In the field of electron microscopy, use has in the past been made of anodic aluminium oxide as a substrate for transmission electron microscopy. After removal from the metal, the oxide is self-supporting in thicknesses down to less than 10nm and is amorphous, so that no appreciable detail is seen in the micrograph or diffraction pattern.

(ii) Sputtering

The method of film deposition, whereby a d.c. glow discharge is established between a plate of source material and the substrate, was used as early as 1842. Many of the interferometer plates used by spectroscopists of the last century were coated by sputtering. Although the experimental arrangements required are simple, the process is a somewhat complex one. Basically removal of the cathode material result from the bombardment of the cathode by energetic positive ions of the discharge. Although there are many features of the sputtering process which remain to be understood, it now seems well established that the removal of cathode material is associated with momentum transfer from the bombarding ions. In simple sputtering, no chemical reactions are involved.

(iii) Thermal evaporation in vacuo

Interest has grown over the past 30 years or so in this method of preparing films. The pressure of gas in a chamber is reduced to as low a value as possible and the source material is heated to a sufficiently high temperature to ensure that evaporation (or sublimation) will occur at a suitable rate. For the purpose of obtaining a 'parallel-sided' film on a plane substrate, it is sufficient to ensure that the pressure of residual gas in the chamber is low enough for the mean free path of the atoms of evaporated material to be larger than the source-substrate distance. In fact, films produced under conditions where this is only marginally satisfied may well show a marked influence of the residual gas in the chamber.

1.5.3. APPLICATION OF THIN FILMS

As has been shown in the foregoing pages, thin films exhibit remarkable optical, electrical, mechanical,, and other properties. In addition thin films may considerably influence various processes occurring at surfaces and interfaces as corrosion friction, catalysts, etc.

(a) Applications of Mechanical Properties

Thin films are used more and more as layers lowering friction, as anti-corrosion coatings and as coatings that considerably reduce the wearing of mechanically loaded parts. In sliding bearings, for example, evaporated iridium thin films are used on account of their lubricating power. Relay contacts are coated with thin films of rare metals in order to prevent burning, etc. Very hard titanium nitride and titanium carbide coatings are used for reduction of friction and extending the life of high-speed steel ools (e.g., lathe tools, tools for tapping carbon steel nuts, etc.). TiN also has interesting optical properties so that it could be used in silicon solar cells as a transparent

conductive material and decorative coating.

(b) Application in Electronics and Microelectronics

The applications of thin films in electronics have been steadily growing in importance during the past years. The construction of digital computers and of other sophisticated electronic systems for measurement or control require a multiple duplication of identical functional elements(e.g., logical circuits, memories, amplifiers, etc.) This evelopment aims at grouping these elements into independent units – integrated circuits – for the production of which thin films are of paramount importance.

CHAPTER 2

EXPERIMENTAL

2.1 CHEMICALS

The chemicals used for preparation are listed below in table 2.1

TABLE 2.1 Chemicals and suppliers

CHEMICALS	SUPPLIER	GRADE
Cobalt acetylacetonate	Aldrich	Analytical
Nickel acetylacetonate	Aldrich	Analytical
Copper acetylacetonate	Aldrich	Analytical
Isopropyl alcohol	Aldrich	Analytical
2-methoxy ethanol	SAARchem	Analytical
Nitrogen gas {N_2}	MG Fedgas	Analytical
Titanium(VI) isopropoxide	Aldrich	Analytical

2.2 GENERAL SCHEMES FOR FILM PREPARATION

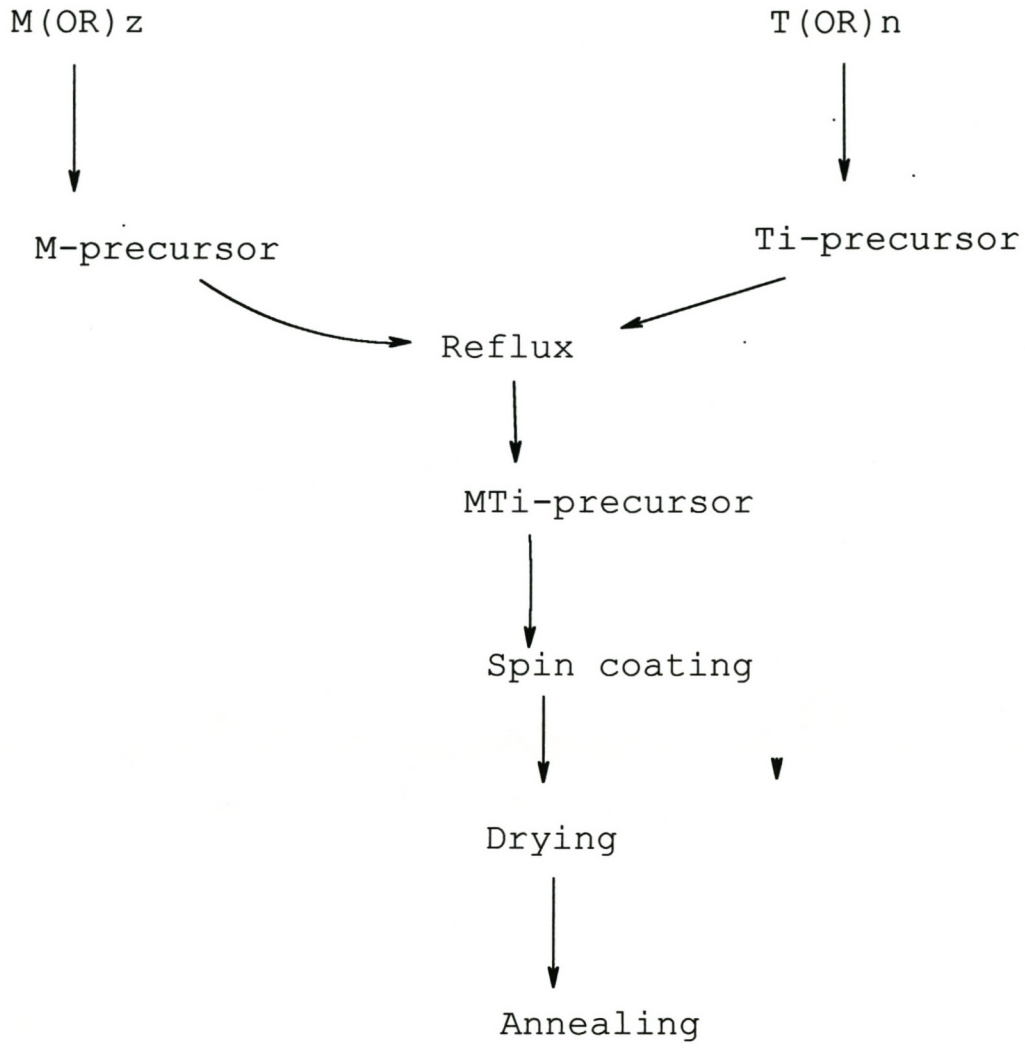

2.3 CHARACTERISATION OF FILMS AND POWDERS

(a) Rutherford Backscattering

The thickness and composition of the films deposited on silicon (Si<100>) wafers were determined by RBS at the National Accelerator Centre (NAC) in Faure. The scattering chamber and the beam lines were evacuated to a vacuum better than 10^{-4} Torr using a forepump and a turbomolecular pump. Monoenergetic and collimated alpha particles (He^+ ions) were accelerated to an energy of 2MeV by a Van de Graaff accelerator and directed through a series of collimators with the last one defining the analysing beam incident on the sample. A final collimator of 1 mm diameter was used for analysis of laser irradiated samples and allowed for precise positioning of the beam onto the laser spot. Backscattered particles were detected with a solid detector, mounted in the plane of the beam at an angle of 165° with respect to the incident beam direction. The detected particles were analysed for energy and stored in a multichannel analyser using an appropriate calibration factor relating channels to energy. A standard Pt_2Si sample was used for calibrations and an energy calibration of 4 KeV per channel was maintained through an analysis run. Final data, stored in the form of a spectrum was then stored in a computer.

(b) Scanning Electron Microscopy

Thin films deposited on Si<100> wafers were mounted on a specimen holder at theUniversity of Stellenbosch. The films were made conductive by pasting a Ag epoxy on the edges of the wafers. The surface morphology studies of the films were carried out on a Hitachi X-650, a 40 KeV machine offering resolution as good as 6nm. The scanning electron microscope uses a focused beam of high-energy electrons that scans across the surface of the specimen when the accelerating voltage lies between 5 – 40 KV. The specimens were scanned by incident electrons and electrons emitted from the surface were collected and amplified for video signals. These signals were stored in a computer.

(c) X-ray diffraction

The x-ray powder diffraction of the metal oxides ($NiTiO_3$ and $CoTiO_3$) was done on a Philips diffractometer at NAC. The diffractometer was arranged such that the sample (powders and thin films) was in the form of a flat plate that rotates within the diffractometer with an increasing angle θ. A counter moved around the diffractometer at twice the speed of the rotating sample so that it always remained at an angle 2θ to the incoming rays. The resultant pattern was then recorded. The phase or phases within the sample were identified by corresponding them to other known patterns found in the Powder Diffraction File.

(d) Atomic Force Microscopy

A Topometrix Explorer TMX 2000 with force spring constant of 35-65N/m was used to determine the surface analysis. The samples were measured in non contact mode with a low resonance cantilever. An atomically sharp tip was scanned over a surface with feedback mechanisms that enable the piezo-electric scanners to maintain the tip at a constant force (to obtain height information), or height (to obtain force information) above the sample surface. Tips used were made from Si_3N_4 and were at the end of a cantilever. AFM measurements were made at room temperature (20 °C). The slope of the retraction force curves in the region where probe and sample are in contact was used to convert the voltage into cantilever deflection.

2.4 ELECTRODE MANUFACTURING.

The electrodes were prepared as follows. The thin films were connected to a copper wire using Ag epoxy. The contact of the copper wire and thin films and the edges of the thin films as well as the back of silicon and titanium substrates were insulated with a nail vanish. The part of the copper that was to be immersed in the solution was sealed in a glass capillary and an epoxy resin was used as sealant. Figure 2.1 below shows a diagram of an electrode.

Figure 2.1 A diagram of an electrode.

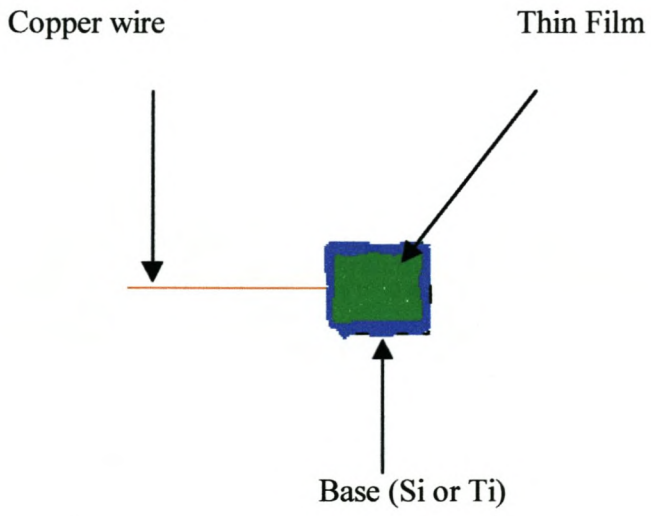

CHAPTER 3

PREPARATION AND CHARACTERIZATION OF $NiTiO_3$ POWDERS AND THIN FILMS

3.1 PREPARATION

3.1.1 SOL GEL PREPARATION OF $NiTiO_3$

Different mole ratios of nickel acetylacetonate to titanium isoproxide as shown in table 3.1, were dissolved in 2-methoxy methanol (20ml) by refluxing and stirring for 2 hrs under a N_2 atmosphere. Titanium isoproxide (1114μl) was dissolved in 2-methoxy methanol (8ml) by refluxing and stirring for 2 hrs under N_2 atmosphere. The two suspensions were added to each other, while stirring and allowed to reflux for 2 hrs. The light green gel was aged in a sealed polypropylene bottle for week.

Table 3.1 Mole ratios of Ni to Ti prepared

Ratios	Ni (mole)	Ti (mole)
1:1	0.005	0.005
0.9:1	0.0045	0.005
0.7:1	0.0035	0.005
0.5:1	0.0025	0.005
0.3:1	0.0015	0.005

3.1.2 PREPARATION OF FILMS AND POWDERS.

(a) Films

The metal oxide ($NiTiO_3$) gels were spin coated 5 times onto different substrates namely: silicon and titanium substrates and then heated at 150°C for 30 minutes to obtain transparent thin films. The films on silicon wafers and on titanium substrates were annealed at 800°C and 400°C respectively under a temperature program in N_2 for 72 hours in order to remove any organic residues.

(b) Powders

The $NiTiO_3$ powders were obtained by evaporating metal oxide gels to dried solid gels, followed by calcination at 400°C and 800°C under N_2 atmosphere. The $NiTiO_3$ powders obtained were yellowish gold colour.

3.2 CHARACTERISATION OF THIN FILMS

3.2.1 STRUCTURAL DETERMINATION

(a) Powder

(i) Thin films and powders of $NiTiO_3$ with different ratios of Ni:Ti were prepared using sol-gel methodology. These powders were calcinated at 400°C and 800°C in order to remove any organic residue and crystallize the final material. The crystalline nature of the powders was identified by x-ray diffraction (XRD). The powders of Ni:Ti were made in the ratios presented in table 3.1. The XRD patterns were recorded on a Philips

diffractometer (using CuKα radiation at 45KV). The post annealing increased the crystallinity of the powders as evidenced by the peak sharpness and intensity in the x-ray diffraction patterns. Table 3.2 is a list of different ratios of Ni to Ti in $NiTiO_3$ extrapolated from XRD results.

XRD reveals that the best route for the preparation of $NiTiO_3$ is involved in low concentration of Ni:Ti, namely is 0.3:1. Table 3.2 shows that all the ratios of Ni to Ti have formed $NiTiO_3$. This is the general trend for the preparation of $NiTiO_3$. The most unsatisfactory route for $NiTiO_3$ preparation was that which involved a high concentration of Ni powders, containing a high impurity of NiO and TiO_2 as compared to others. As the concentration of Ni to Ti was reduced, the NiO formed decreased up to a point where there was no NiO. This was at the ratio of 0.3:1. In the case of the TiO_2 formed, the TiO_2 phase disappeared at ratios 0.5 – 0.3:1Ni:Ti. This could be attributed to the vacancy in the Ni metal.

Table 3.2 The composition and XRD features of Ni:Ti

Ni/ Ti ratios	FEATURES OF XRD		
	Impurity NiO formed	Impurity TiO_2 formed	Main feature $NiTiO_3$ formed
1:1	Yes	Yes	Yes
0.9:1	Yes	Yes	Yes
0.7;1	Yes	Yes	Yes
0.5:1	Yes	No	Yes
0.3:1	No	No	Yes

Figures 3.1 and 3.2 show the XRD patterns of 0.3:1 and 0.5:1 powders respectively.

Figure 3.1: XRD spectrum of $NiTiO_3$ with low loading of 0.3:1Ni:Ti

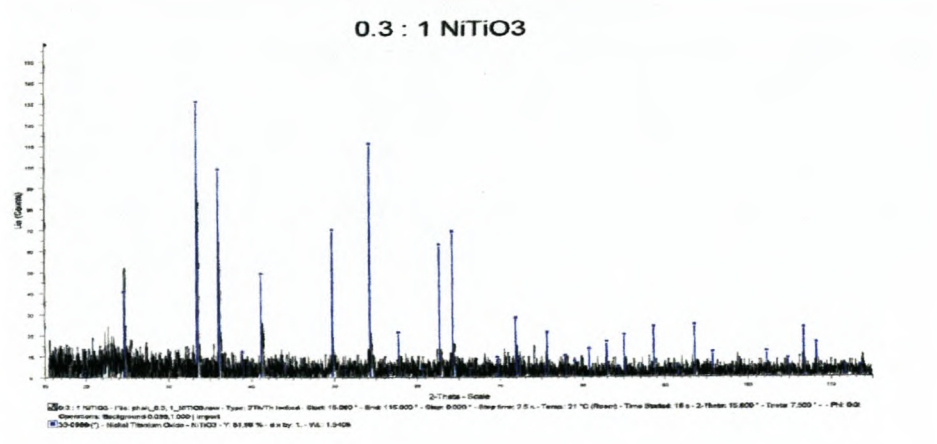

Figure 3.2: XRD spectrum of $NiTiO_3$ with high loading of 0.5:1Ni:Ti

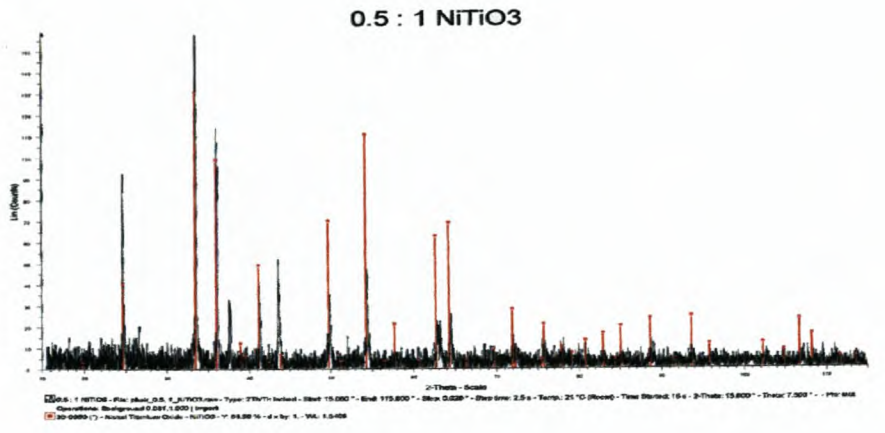

The XRD pattern of 0.3:1 $NiTiO_3$ in figure 3.1 shows a well–crystallized nature of the formed metal oxide. It matches with the JCPDS standard 33-0960 for rhombohedral $NiTiO_3$ structure. Figure 3.2 is the XRD spectrum of $NiTiO_3$ where the Ni loading is 0.5 with respect to Ti. The diffractogram shows well-defined peaks, showing a good crystallinity. The θ values and intensities of the peaks agree very well with those given in JCPDS standard 33-0960 (red pattern) for $NiTiO_3$, suggesting that the powder is a perovskite structured material that has a rhombohedral phase. It also shows peaks of a NiO impurity that matches with the JCPDS standard 78-0429 (green pattern) of cubic NiO. The structure of the rhombohedral oxide consists of a hexagonal close packed oxygen array with two thirds of the octahedral interstices occupied to give the general formula: ABO_3 where the octahedral A-sites are occupied by Ni(2+) and B by Ti(4+). The rhombohedral oxides are in the hexagonal crystal system (trigonal sub-system) and

are consequently uniaxial with the exception of corundum, which is colorless (see below), these minerals are all opaque in thin section. The mineral examples in this group are included: in table 3.3.

Table 3.3: Examples of Rhombohedral Oxides

Name	Formula
Corundum	Al_2O_3
Hematite	Fe_2O_3
Ilmenite	$FeTiO_3$
Geikielite	$MgTiO_3$
Pyrophanite	$MnTiO_3$

It was found that the preferred structure of $NiTiO_3$ is in a ratio of Ni:Ti of 0.3:1 (50).

(b) Thin Films

Thin films of $NiTiO_3$ were prepared in the similar way to the powders. Analysis by XRD revealed that the films could be amorphous because the strong peaks of the crystalline phases were not present on the film patterns. It could also be due to weak signals obtained from the thickness of the films, thus not diffracting enough.

3.2.2 SURFACE ANALYSIS

(a) SEM

Surface morphology studies of the films were carried out on a Hitachi X-650, a 40 KeV machine offering resolution as good as 6nm. Thin films were deposited on the silicon and titanium substrates. They were dried and annealed under the same conditions. Figure 3.3

show a scanning electron micrograph of a $NiTiO_3$ thin film deposited on silicon wafer. The micrograph of 0.5:1Ni:Ti in $NiTiO_3$ shows that the film in figure 3.3 consists of a continuous layer and non-homogeneous distributed small grains. It also shows that the film is smooth, uniform and crack-free. Figure 3.4 shows a scanning electron micrograph of a $NiTiO_3$ thin film deposited on a titanium substrate. Figure 3.4 reveals that the particles on the surface of the film are arranged in a regular manner and that there are no apparent holes present at the observed magnification. This is indicative of fairly smooth film formation.

Figure 3.3 A Scanning electron micrograph of 0.5:1Ni:Ti in $NiTiO_3$ on a silicon substrate with magnification of 500x, 25KV and 20.0μm bar

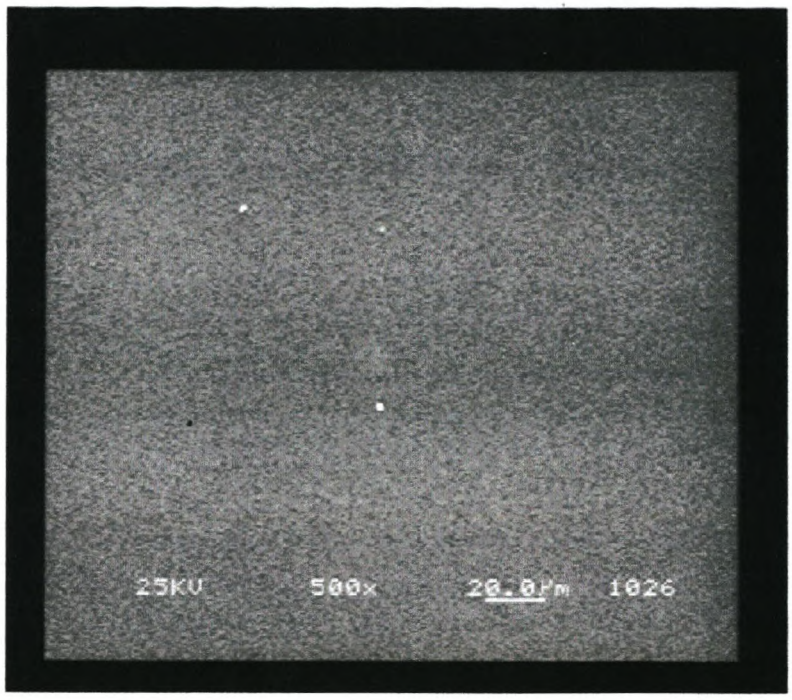

Figure 3.4: A Scanning electron micrograph of $0.5{:}1NiTiO_3$ on a titanium substrate with magnification of 500x, 25KV and 20.0μm bar

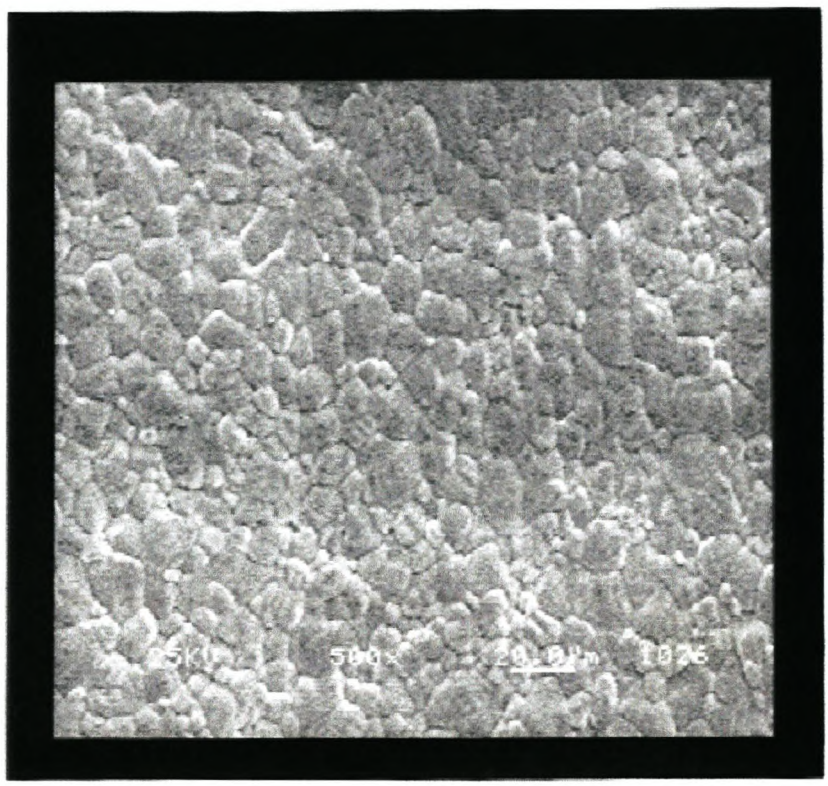

(c) AFM Analysis

A Topometrix Explorer TMX 2000 with force spring constant 35-65N/m was used to determine the surface analysis. The samples were analysed in non-contact mode, with a low-resonance cantilever. Figures 3.5 3.6 and 3.7 below are the spectra of ratios of Ni:Ti of 0.3:1, 0.5:1 and 0.7:1 respectively. These thin films were deposited on a silicon substrate. Table 3.4 is a list of thin film composition, their roughness and particle size.

Table 3.4: Composition of thin films, roughness and particle size

$NiTiO_3$	Roughness Ra(nm)	Particle size (nm)
0.7:1	6.47	220 – 250nm
0.5:1	9.37	200 – 300nm
0.3:1	104.94	200nm

Table 3.4 represents the results that were interpreted from analysis by AFM. It shows that as the concentration of Ni:Ti is reduced, the roughness of the thin film increases. The quantification of the "quality" is in terms of certain light scattering criteria (51) or surface roughness values using sensitive instrumental techniques (52) becomes increasingly critical for very low scatter optics and coatings (< 10 ppm of total integrated scattering). The particles are arranged in a regular manner as shown in figures 3.5 – 3.7 and the particle size varies from 200nm to 300nm. The 0.7:1Ni:Ti in $NiTiO_3$ has a smoother surface than films prepared with a low concentration of Ni:Ti. This result is in agreement

with the SEM, XRD and RBS results, which suggests that films with a lower Ni loading form the $NiTiO_3$ phase.

Figure 3.5: Atomic force micrograph of 0.3:1 $NiTiO_3$ on silicon substrate with (area 5μm x 5μm)

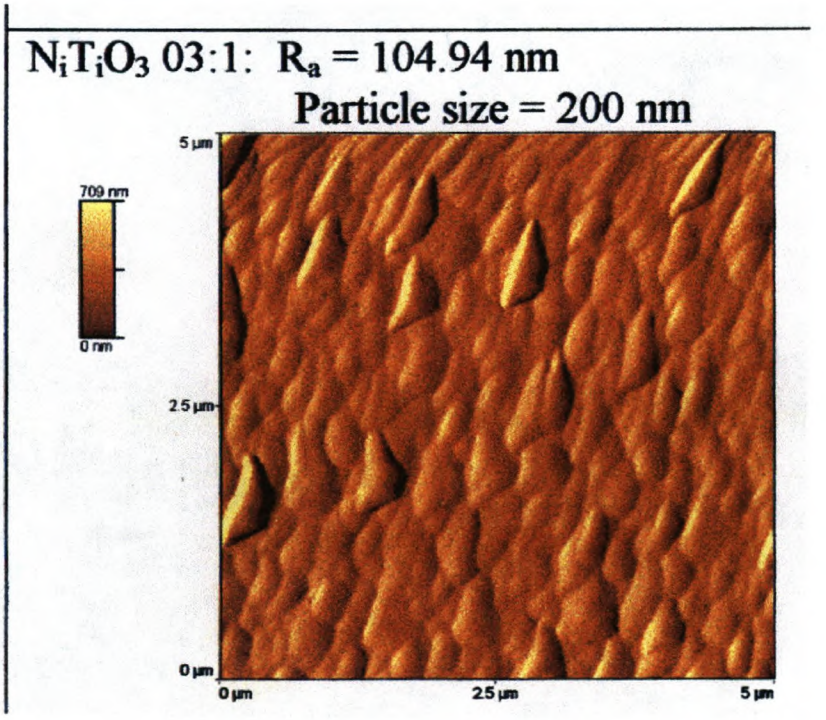

Figure 3.6: Atomic force micrograph of 0.5:1 $NiTiO_3$ on silicon substrate with (area 5μm x 5μm)

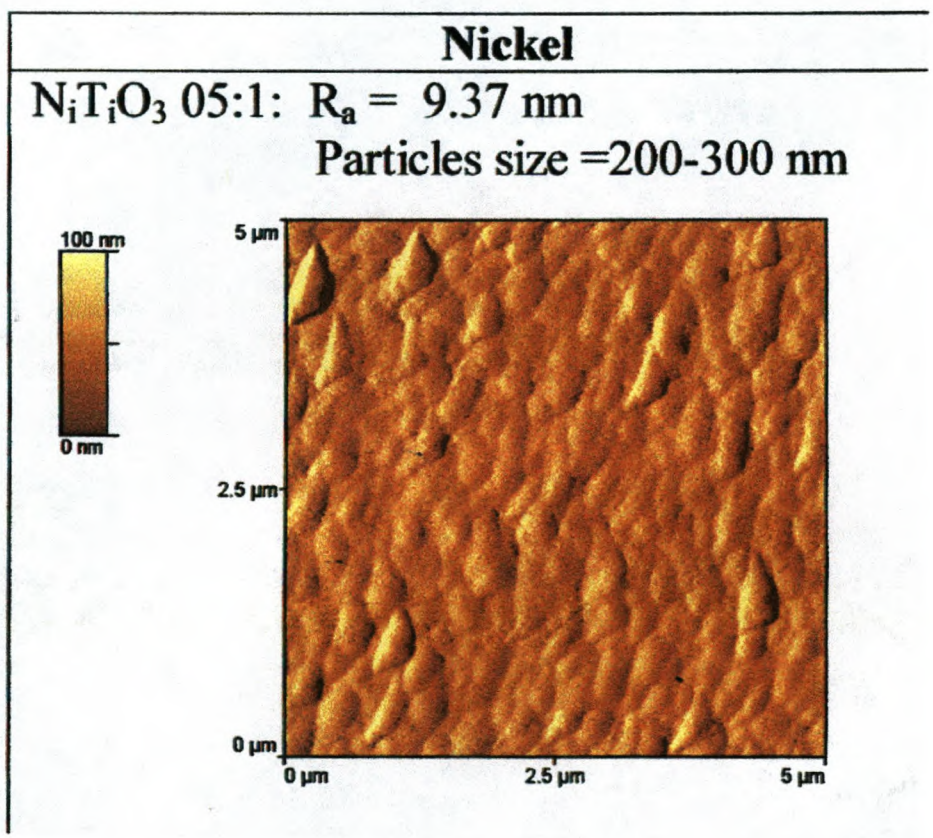

Figure 3.7: Atomic force micrograph of 0.7:1 $NiTiO_3$ on silicon substrate with (area 5μm x 5μm)

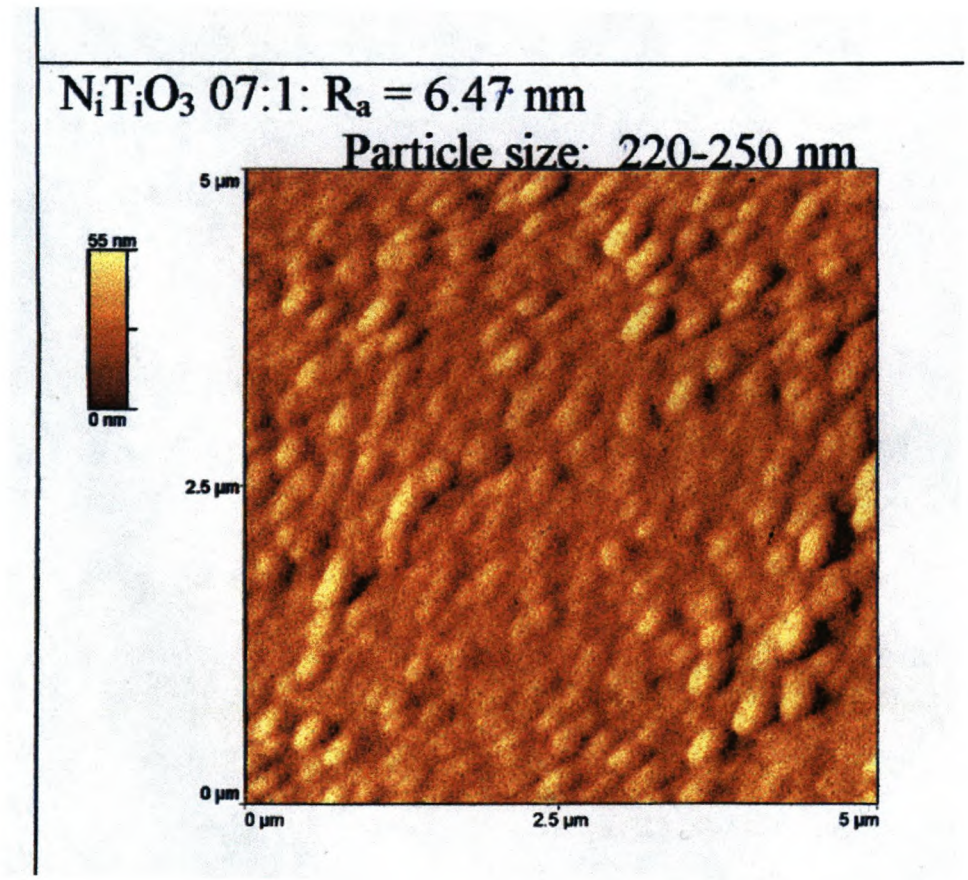

3.2.3 DETERMINATION OF COMPOSITION

Rutherford backscattering spectroscopy is a technique used to determine the stoichiometry and thickness of thin films. The thickness and composition of the films deposited on silicon and titanium substrates were determined by RBS at the National Accelerator Centre (NAC). Figure 3.8 below shows the RBS spectra of a 0.3:1 and 0.5:1Ni:Ti in $NiTiO_3$ thin film deposited on silicon wafers. The 0.3:1 and 0.5:1Ni:Ti were labeled by Kobe 1006 and 1008 respectively. It shows that the peaks were identified to be O, Ti and Ni. For the Si substrate, the expected signal will be a slightly less than what was found. The shift is due to SiO_2 layer formed underneath the metal titanate layer during the annealing process. Since the peaks of Ti and Ni are well separated, the area density of each component can be calculated by integration.

Figure 3.8: Rutherford backscattering spectra of 0.3:1 and 0.5:1Ni:Ti in $NiTiO_3$ on a silicon substrate

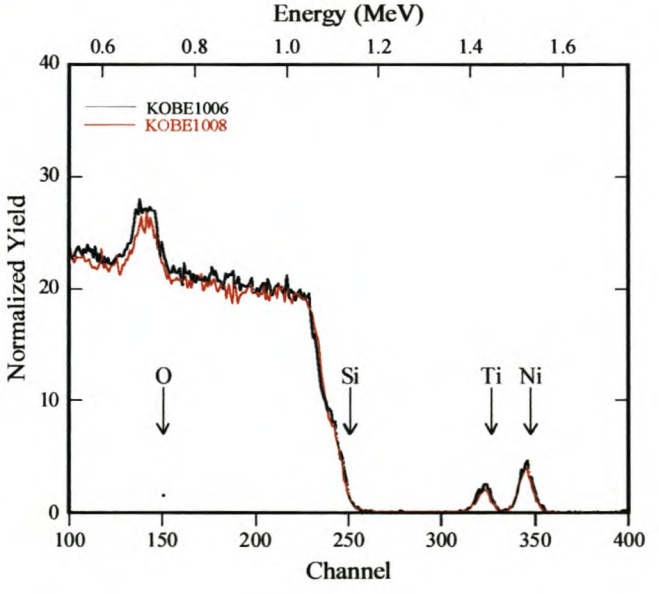

Figure 3.9: Rutherford backscattering spectra of 0.3:1 and 0.5:1Ni:Ti in $NiTiO_3$ on a silicon substrate

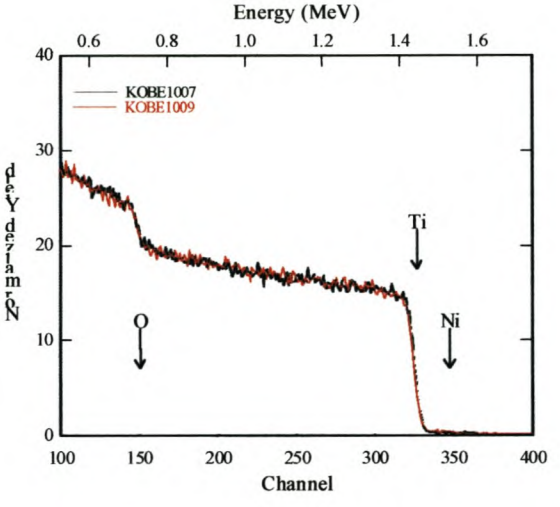

The thickness and the composition were determined by using the Rutherford Universal Manipulation Program (RUMP) (53). As the O signal sits on top of the Si substrate signal, there is a larger uncertainity in its determination due to the uncertainity of the background signal. Table 3.5 shows the composition and the thickness of the $NiTiO_3$ films. From the table it is noticed that films with M_xTiO_y, where x = 1 were prepared and characterized.

Table 3.5: The composition and thickness of $NiTiO_3$ films

File name	Ni_xTi	Film thickness (nm) ± 5nm	Ni	Ti	O	synthesis Ni/Ti
kobe 1008	x = 0.5	10	1.08	1	3.06	0.5:1
kobe 1006	0.3	11	1.08	1	3.06	0.3:1

The values of M; Ti and O_y were obtained by simulation of peaks give the ratio of M:Ti and O_y:Ti. The thickness of the $NiTiO_3$ films vary from 10 nm to 11 nm. The RBS spectrum of all metal titanates shows two layers, the first is of $NiTiO_3$ and the other layer is the base SiO_2 as shown in figure 3.8. This is due to the formation of a barrier SiO_2 layer. The oxygen has diffused to the silicon substrate during the high temperature annealing.

RBS spectra of $NiTiO_3$ films deposited on titanium substrate are shown in figure 3.9. RBS reveals that metal titanates could not be detected. This means that the metal titanate layer was lost or completely destroyed during the high annealing process as shown in figure 3.9 Figure 3.9 shows the RBS spectra of a 0.3:1 and 0.5:1Ni:Ti in $NiTiO_3$ thin film deposited on titanium substrate. The 0.3:1 and 0.5:1Ni:Ti were labeled by Kobe 1007 and 1009 respectively. RBS shows that the Ni has completely disappeared from the titanium matrix. It also shows that the TiO_2 layer that formed is approximately more than 1000nm.

RBS reveals that for $NiTiO_3$ thin films irrespective of whatever ratio, the most favourable ratios of these metal titanates is in a ratio of 1 to 1 Ni:Ti. The oxygen content is highly variable because analysis by RBS is not ideal for light elements.

3.2.4 CHECKING OF ORGANIC RESIDUES.

Figure 3.10 shows the FTIR spectra of 0.3:1; 0.5:1 and 0.7:1 Ni:Ti in $NiTiO_3$ powders. The spectra show no C-H and C-O stretching peaks. This implies that the organic tail (isopropoxide) had been decomposed. The band at 3451cm^{-1}: 2363-2345cm^{-1} and 1870-1320cm^{-1} are due to air. The strong bands between 800 and 400cm^{-1} are mainly due to the formation of metal oxides (M-O: NiO and TiO) (54).

Figure 3.10: FTIR spectra of 0.3:1, 0.5:1 and 0.7:1Ni:Ti in $NiTiO_3$

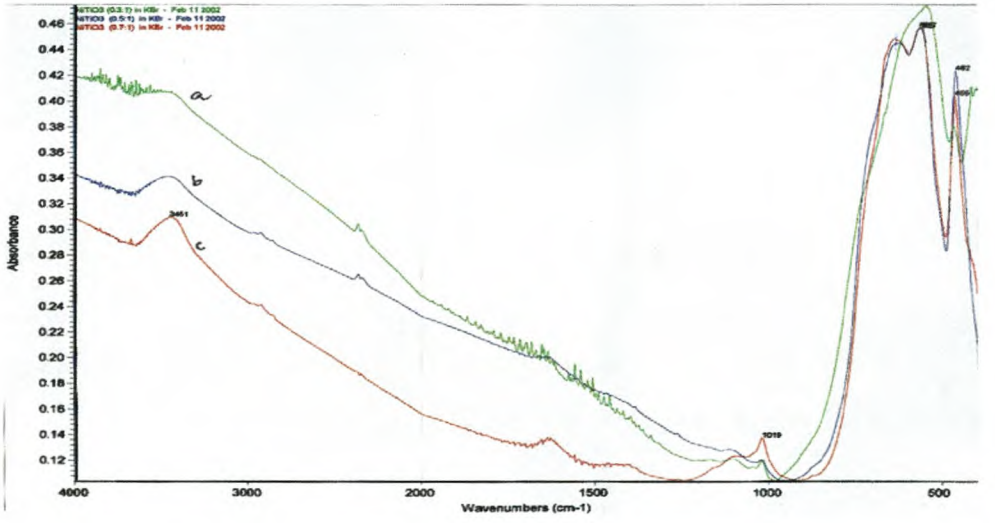

The band due to the Ti-O stretching vibration has been found near the region of about 1091cm^{-1}. As the concentration of Ni to Ti is reduced, the TiO_2 is also decreased. At low concentration of 0.3:1 Ni :Ti, there is a broad single peak near the region of 800-500cm^{-1}, while the other ratios have formed two peaks in this region. This is attributed to the presence of NiO present and it is confirmed by XRD. The NiO band is near the region

$800cm^{-1}$-$700cm^{-1}$. Infrared absorption bands have been observed in the vicinity of 500 to $600cm^{-1}$ and 350 to $400cm^{-1}$ for various titanates investigated in tabe 3.6 (49).

Table 3.6: Absorption-band centres.

Metal titanate	v_1 (cm^{-1})	V_2 (cm^{-1})
$BaTiO_3$ (cubic)	495	
$BaTiO_3$ (rhombohedral)	532; 490	
$BaTiO_3$ (hexagonal)	555	365
$SrTiO_3$ (cubic)	610	395
$CaTiO_3$ (orthorhombic)	540; 700 (shoulder)	360

FTIR reveals that for rhombohedral phase, the observed twin peak are at 557 and $650cm^{-1}$ respectively.

3.3 CONCLUSIONS

Thin films and powders with different preparative stiochiometry of nickel titanium oxide were prepared by using the sol-gel technique. The surfaces were all annealed at 400°C and 800°C under a temperature program in order to remove any organic residues The crystalline nature of the powders was identified by X-ray diffraction. XRD shows that all the ratios of Ni to Ti (0.3,0.5,0.7,0.9 and 1;1) have formed $NiTiO_3$ powder. The best method for $NiTiO_3$ preparation is at the low concentration of 0.3:1Ni:Ti. Thin films could not be detected because they could be amorphous. SEM has shown that the $NiTiO_3$ film surface deposited on the silicon substrate is smooth, uniform and crack-free. AFM studies show that as the concentration of Ni:Ti is reduced, the roughness of the thin film increases. The 0.7:1 $NiTiO_3$ has a smoother surface than the films prepared with lower ratios of Ni:Ti. SEM, XRD, FTIR and RBS suggest that the 0.3:1 and 0.5:1Ni:Ti films have the same $NiTiO_3$ structure, with 10nm and 11nm thickness, respectively.

CHAPTER 4

PREPARATION AND CHARACTERIZATION OF $CoTiO_3$ MATERIALS

4.1 PREPARATION

4.1.1 SOL GEL PREPARATION OF $CoTiO_3$

Different ratios of cobalt acetylacetonate to titanium isopropoxide as tabulated in table 4.1 were dissolved in 2-methoxy ethanol (20ml) and refluxed under inert conditions for 2 hours.Titanium isopropoxide was also dissolved in 2-methoxy ethanol (8ml) and refluxed under inert conditions for 2 hours. These two suspensions were then added to each other, while stirring, and allowed to reflux for 2 hours. The dark greenish / grey gel was aged in a sealed polypropylene bottle for one week.

Table 4.1 Mole ratios of Co to Ti prepared

Ratios	Co (mole)	Ti (mole)
1:1	0.005	0.005
0.9:1	0.0045	0.005
0.7:1	0.0035	0.005
0.5:1	0.0025	0.005
0.3:1	0.0015	0.005

4.1.2 PREPARATION OF FILMS AND POWDERS.

(a) Films

The $CoTiO_3$ gels were spin coated 5 times onto different substrates namely: silicon and titanium substrates and then heated at 150°C for 30 minutes to obtain transparent thin films. The films on silicon wafers and on titanium substrates were annealed at 800°C and 400°C respectively under temperature program in N_2 for 72 hours in order to remove any organic residues.

(b) Powders

The powders were obtained by evaporating the metal oxide gels to dried solid gels, followed by calcination at 400°C and 800°C under N_2 atmosphere. $CoTiO_3$ powders with a dark grey colour were obtained.

4.2 CHARACTERISATION OF THIN FILMS

4.2.1 STRUCTURAL DETERMINATION

(a) Powder

Powders of $CoTiO_3$ were prepared in the same way as with the $NiTiO_3$ powders. Table 4.2 shows results that were interpreted from XRD analysis.

Table 4.2 The composition and XRD features of Co:Ti

Co/ Ti ratios	FEATURES OF XRD			
	Impurity $CoCo_2O_4$ formed	Impurity TiO_2 formed	Co_2TiO_4 formed	Main feature $CoTiO_3$ formed
1:1	No	No	Yes	No
0.9:1	No	No	Yes	No
0.7;1	Yes	Yes	Yes	No
0.5:1	Yes	No	No	Yes
0.3:1	Yes	Yes	No	Yes

High Co concentrations, ranging from 1:1 to 0.7:1Co:Ti, forms the cubic phase with Co_2TiO_4 structure as tabulated in table 4.2. This is expected due to the high concentration of Co loading. Low Co concentration ranging, from 05:1 to 0.3:1, a rhombohedral phase with $CoTiO_3$ structure is formed as tabulated in figure 4.2. The best route for $CoTiO_3$ formation is at 0.5:1Co:Ti. The product contains $CoCo_2O_4$ impurity however. Fine adjustments of the ratios are needed for $CoTiO_3$ formation.

Figure 4.1: XRD spectrum of $CoTiO_3$ with 05:1Co:Ti.

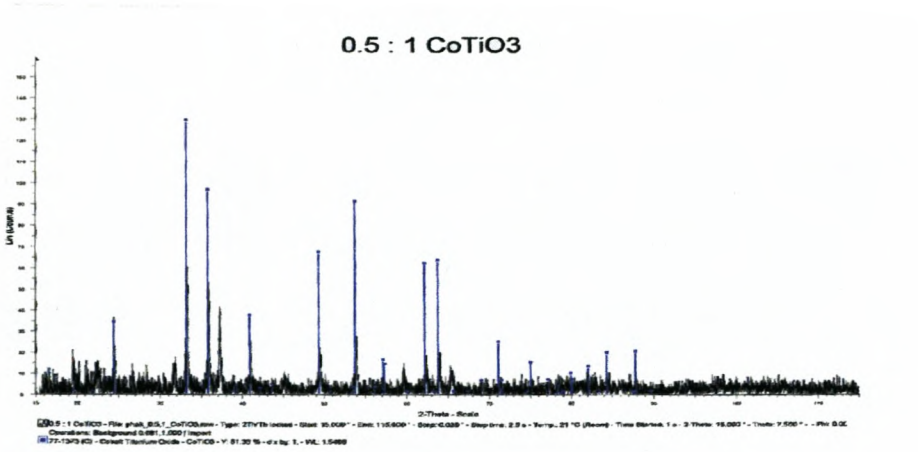

Figure 4.2: XRD spectrum of Co_2TiO_4 with 1:1Co:Ti

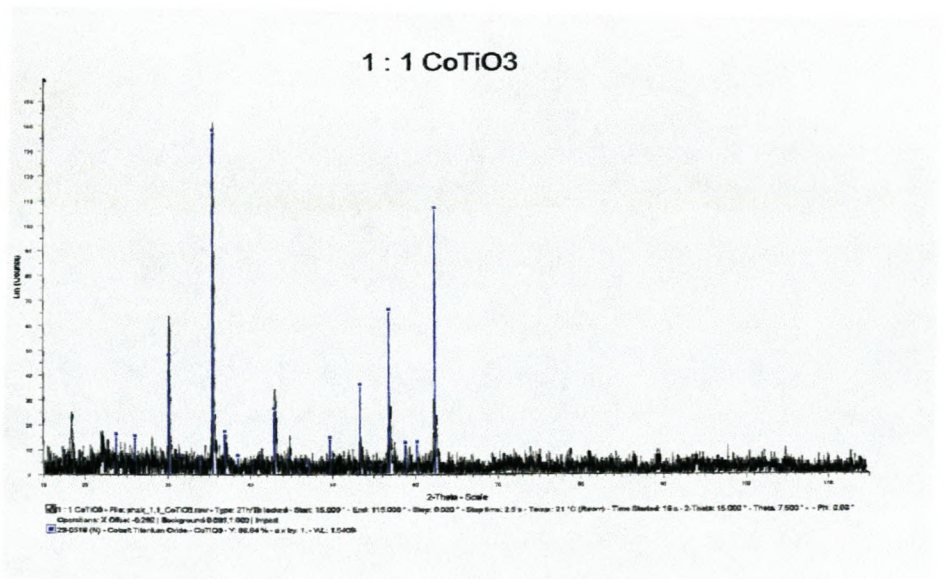

The XRD spectrum of the 0.5:1 $CoTiO_3$ powder in figure 4.1 above shows well defined peaks that indicate a high degree of crystallinity. It corresponds with the JCPDS standard 15-0866 (blue pattern) rhombohedral $CoTiO_3$ structure. It also shows impurities of $CoCo_2O_4$ in figure 4.1. Figure 4.2 above shows a XRD pattern of Co:Ti powder in a ratio of 1:1. It matches with the JCPDS standard 39-1410 (red pattern) cubic Co_2TiO_4 (50).

(b) Thin Films

Thin films of $CoTiO_3$ were prepared in the similar way to the powders. The XRD analysis reveals that the films could be amorphous because the strong peaks of the crystalline phases are not present on the film patterns.

4.2.2 SURFACE ANALYSIS

(a) SEM

Surface morphology studies of the films were carried out on a Hitachi X-650. Thin films were deposited on silicon and titanium substrates. They were dried and annealed under the same conditions as described in chapter3 for $NiTiO_3$ films. Figures 4.3 and 4.4 show scanning electron micrographs of $CoTiO_3$ and Co_2TiO_4 thin films deposited on silicon wafers respectively. Figure 4.3 shows that the 0.5:1Co:Ti in $CoTiO_3$ is rough with cracks. This could be attributed to the stresses resulting from film-substrate. Gels with different pore size are easily cracked during drying. According to K. H Guenther (55) only gel films with a thickness less than 1μm can be dried on a substrate without cracking. It also has distributed grains that could be due to $CoCo_2O_4$ formed. Figure 4.4 of a 1:1Co:Ti film shows that the surface of the film consists of a continuous layer and non-homogeneous distributed small grains with cracks. Certain parts of the surface are circle-shaped and could be attributed to the spinning process.

Figures 4.5 and 4.6 show scanning electron micrographs of $CoTiO_3$ and Co_2TiO_4 thin films deposited on titanium substrate respectively. Figure 4.5 of 0.5:1Co:Ti in $CoTiO_3$ reveals that the film is crack-free. There are crystal particles on the surface of the film that are arranged in a regular pattern. The 1:1Co:Ti in figure 4.6 shows that the crystal particles are arranged in a uniform way and no holes are present.

Figure 4.3: A Scanning electron micrograph of $CoTiO_3$ with magnification of 200x, 25KV and 50.0μm bar

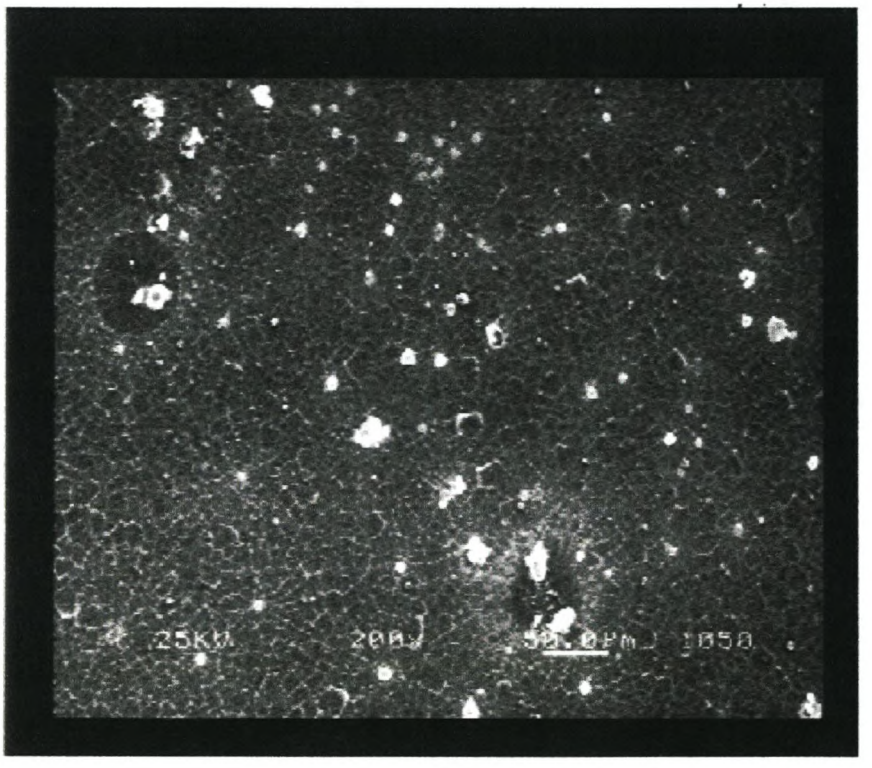

Figure 4.4: A Scanning electron micrograph of Co_2TiO_4 with magnification of 200x, 25KV and 50.0μm bar

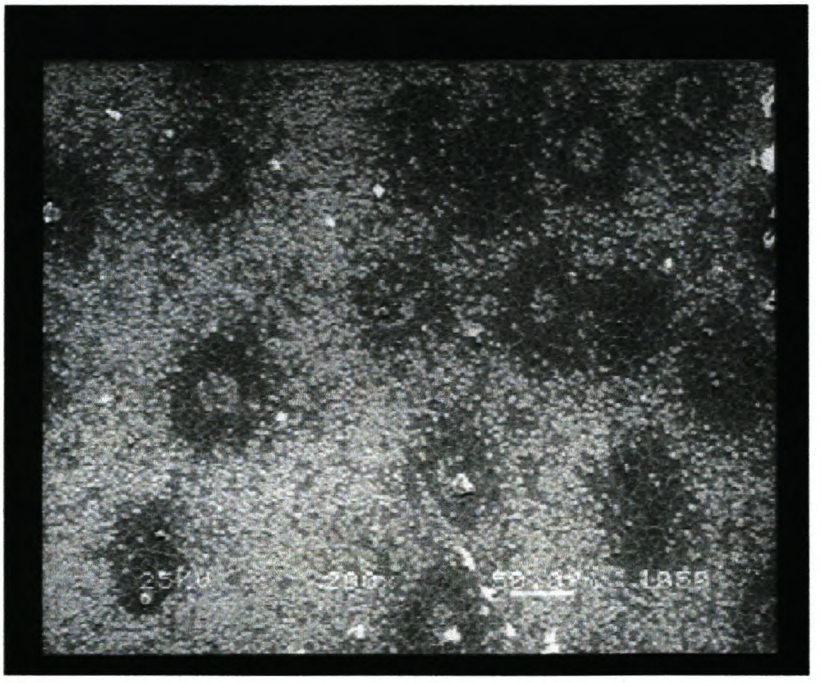

Figure 4.5: A Scanning electron micrograph of 0.5:1 $CoTiO_3$ on titanium substrate with magnification of 200x, 25KV and 50.0μm bar

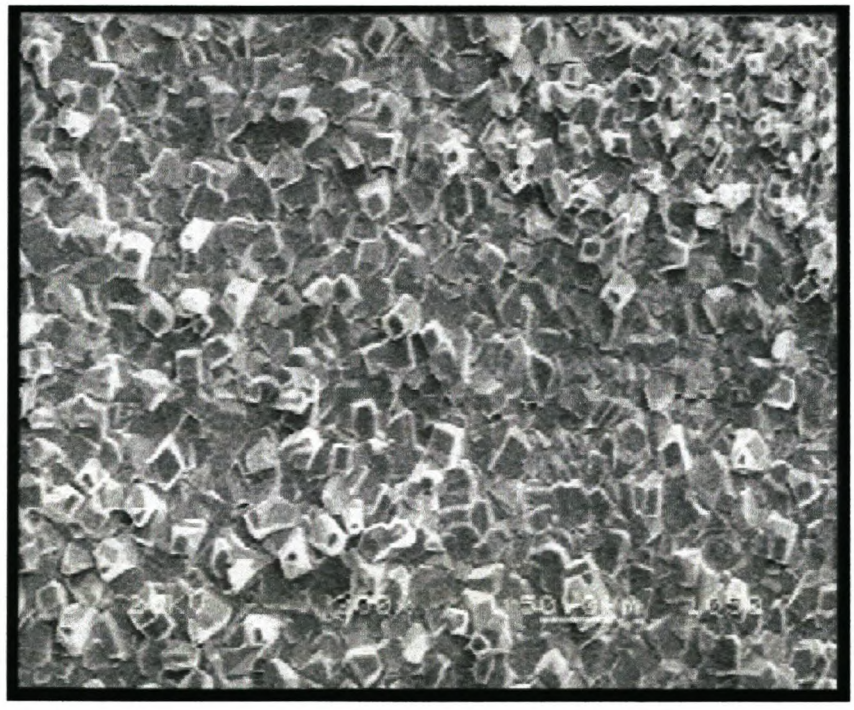

Figure 4.6: A Scanning electron micrograph of 1:1 Co:Ti on titanium substrate with magnification of 200x, 25KV and 50.0μm bar

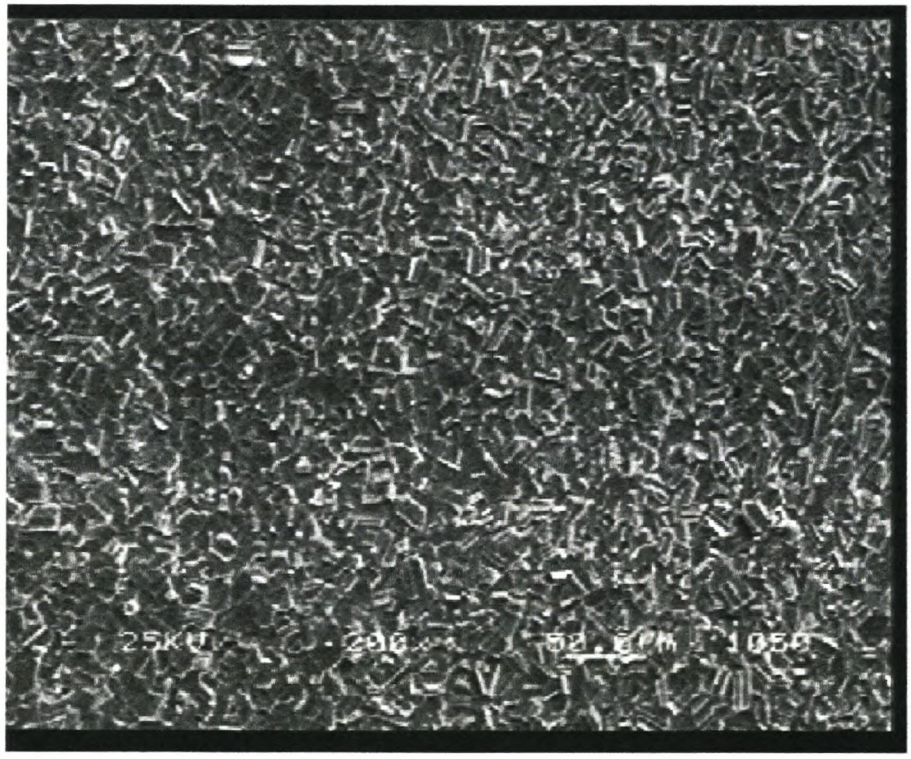

(b) AFM Analysis

A Topometrix Explorer TMX 2000 with force spring constant 35-65N/m was used to determine the surface analysis of $CoTiO_3$ films. The samples were analysed in non-contact mode with a low resonance cantilever. Figures 4.7 and 4.8 below are the spectra of 0.5:1:1 and 1:1Co:Ti thin films deposited on silicon substrate. Table 4.3 is a list of thin film composition, roughness and particle size of thin films.

Table 4.3: Composition of $CoTiO_3$thin films, roughness and particle size

$CoTiO_3$	Roughness Ra(nm)	Particle size (nm)
1:1	141.87	0.6 - 1μm
0.5:1	23.20	400nm

Table 4.3 represents the results that were interpreted from AFM. It shows that higher concentrations of Co are linked to greater roughness of the surface. The 1:1 Co:Ti has a rough surface compared to the 0.5:1Co:Ti. This is because the two cobalt titanates have different crystal structures. The 0.5:1Co:Ti has a rhombohedral phase and the 1:1Co:Ti has a cubic phase. Surface Analysis by AFM confirms that these cobalt titanates have two phases. The 0.5:1 Co:Ti has triangle-like particles which are organized in a regular manner as shown in figure 4.7 while the 0.7:1 has rod-like particles, as shown in figure 4.8. The 1:1 Co:Ti has a large particle size of 0.6nm to 1μm while the 0.5:1 Co:Ti has a small particle size of 400nm. The AFM results agree with XRD results, showing that these cobalt titanates have different phases.

Figure 4.7: Atomic force micrograph of 0.5:1 $CoTiO_3$ on silicon substrate (Area 5μm x 5μm)

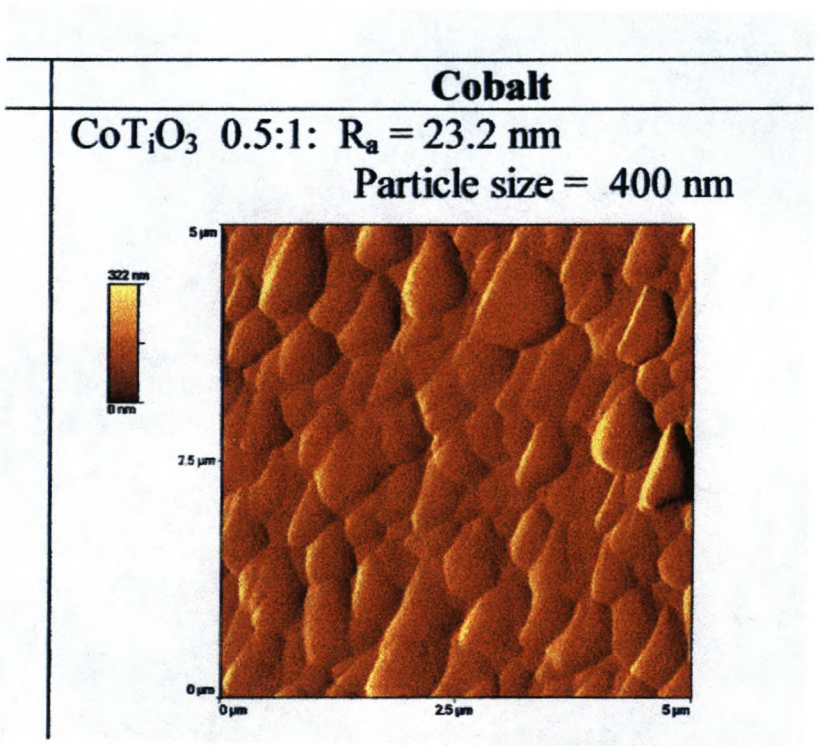

Figure 4.8: Atomic force micrograph of 1:1 $CoTiO_3$ on silicon substrate (Area 5μm x 5μm)

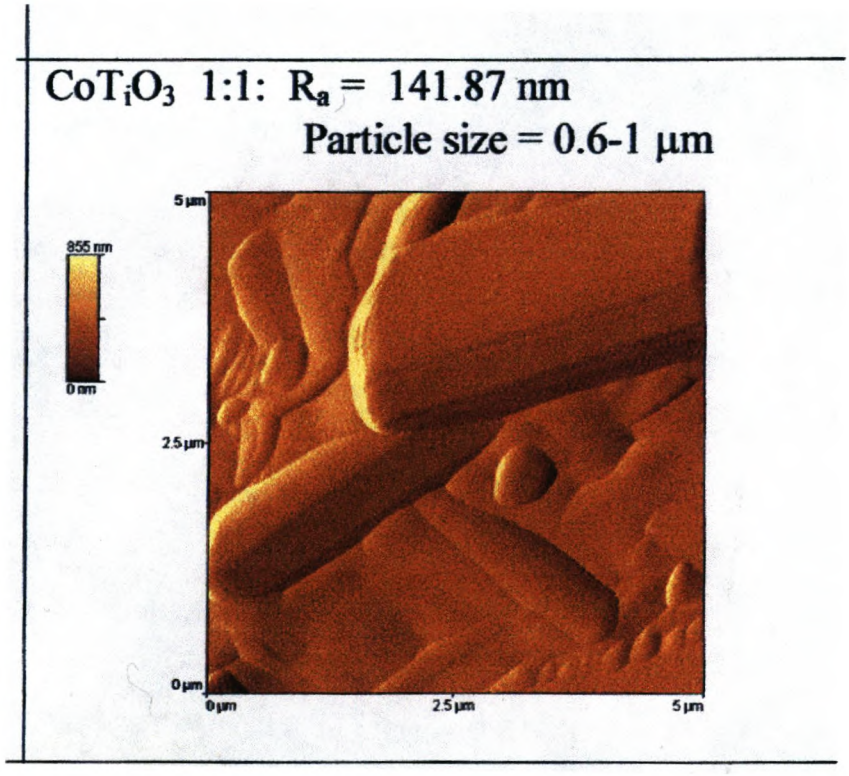

4.2.3 DETERMINATION OF COMPOSITION

Figures 4.9 and 4.10 below are the RBS spectra of cobalt titanates and $Co_{1.17}TiO_{2.29}$ thin films deposited on silicon wafers.

Figure 4.9: Rutherford backscattering spectrum of $CoTiO_3$

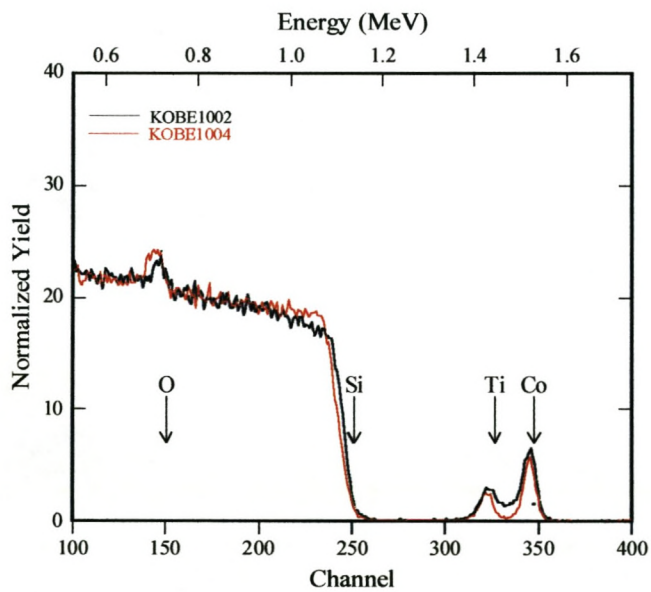

Figure 4.10: Rutherford backscattering spectrum of $Co_{1.17}$ Ti $O_{4.2}$

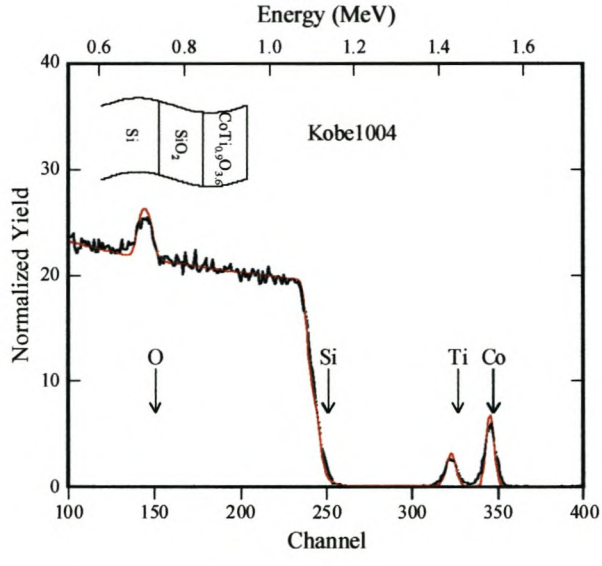

Figure 4.9 below shows the RBS spectra of a 1:1 and 0.5:1Co:Ti in $CoTiO_3$ thin film deposited on silicon wafers. The 1:1 and 0.5:1Co:Ti were labeled by Kobe 1002 and 1004 respectively. For the Si substrate, the expected signal is a slightly less than what was found. The shift in the signal is due to SiO_2 layer formed underneath the metal titanate layer during the annealing process. Since the peaks of Ti and Co are well separated, the area density of each component can be calculated by integration. Stimulation of 1:1 and 0.5:1Co:Ti in figure 4.9 reveal that a SiO_2 layer is formed underneath the $CoTiO_{2.29}$. O, Ti and Co peaks were identified, showing that the structure has O, Ti, and Co present.

The thickness and the composition of cobalt titanates were determined by using Rutherford Universal Manipulation Program (RUMP) (51). As the O signal sits on top of the Si substrate signal, there is a larger uncertainity in its determination due to the uncertainity of the background signal. Table 4.4 shows the composition and the thickness of the films. From the table it is noticed that films with M_xTiO_y, where x = 1, were prepared and characterised.

Table 4.4: The composition and thickness of $CoTiO_3$

File name	Co_xTi	Film thickness (nm) ± 5nm	Co	Ti	O	synthesis Co/Ti
kobe 1004	x = 1	16	1.17	1	2.29	1:1
kobe 1002	0.5	13	1.39	1	4.2	0.5:1

The values of M; Ti and O_y were obtained by simulation of peaks give the ratio of M:Ti and O_y:Ti. The thickness of the $CoTiO_3$ films vary from 13 nm to 16 nm. The RBS spectrum of all metal titanates shows two layers, the first is of $CoTiO_3$ and the other layer is the base SiO_2 as shown in figure 4.9 and 4.10. This is due to the formation of a barrier SiO_2 layer. The oxygen has diffused to the silicon substrate during the high temperature annealing. The simulation of Ti-O-Co/Si as shown in figure 4.9 and 4.10 reveals that the ratios of Co:Ti is 1:1.

RBS spectra of Co_2TiO_4 and $CoTiO_3$ thin films deposited on a titanium substrate are shown in figure 4.11. Figure 4.11 is a spectra of 1:1 and 0.5:1 of Co:Ti ratios which were labeled by Kobe 1003 and1005 respectively. RBS reveal that metal titanate could not be

detected for Kobe 1005 in figure 4.11. This means that the metal titanate layer was lost or destroyed during the high annealing process as shown below in figures 4.11. Kobe 1003

Figure 4.11: Rutherford backscattering spectrum of $Co_{0.28}TiO_{1.46}$

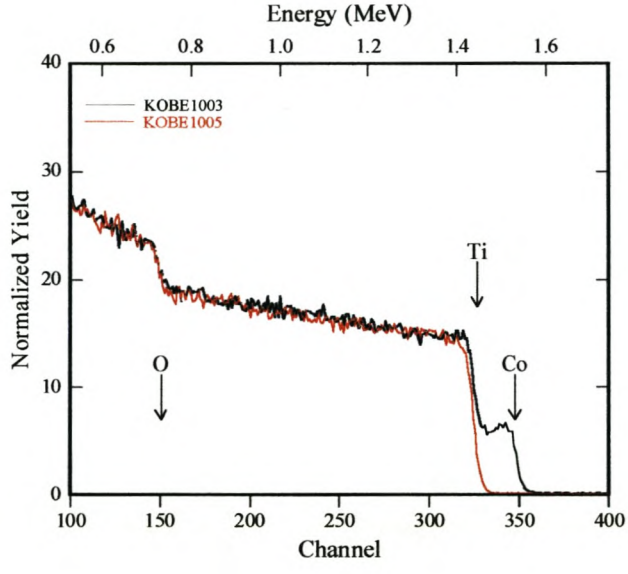

in figure 4.11 is the onlyone that shows the metal titanate layer. The Co, Ti and O peaks were identified, suggesting that Co, Ti and O were present in the structure. $Co_{0.28}TiO_{1.46}$ has a layer of TiO_2 that is greater than 1000nm. The film composition is $Co_{0.28}$ $TiO_{1.46}$ and the thickness is ~ 100nm..

For cobalt titanates thin films, irrespective of their ratio, the most favourable ratio of these metal titanates is 1 to 1 for M:Ti where M is Ni and Co. The oxygen content is highly variable because analysis by RBS is not ideal for light elements.

4.2.4 CHECKING OF ORGANIC RESIDUES.

Figure 4.12 shows the FTIR spectra of 0.5:1 and 1:1 Co:Ti in $CoTiO_3$ powders. The spectra show no C-H and C-O stretching peaks. This implies that the organic tail (isopropoxide) had been decomposed. The band at 3451cm^{-1}: 2363-2345cm^{-1} and 1870-1320cm^{-1} are due to air. The strong bands between 800 and 400cm^{-1} are mainly due to the formation of metal oxides (M-O: NiO and TiO) (54).

Figure 4.12: FTIR spectra of 0.5:1 and 1:1Co:Ti in $CoTiO_3$

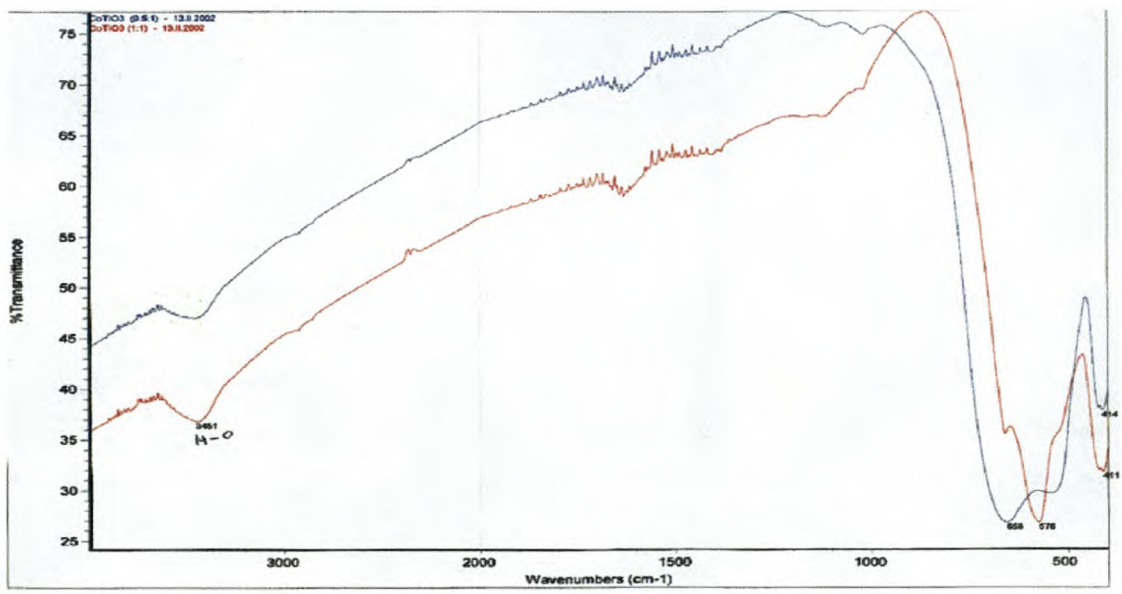

The 1:1 Co:Ti spectrum shows a strong single peak in the vicinity of 800 to 500cm^{-1}. Normally, the cubic phases give a single peak in this region. This is in agreement with XRD results showing that the 1:1 Co:Ti has formed a cubic phase. As the concentration of Co to Ti is reduced, the phase changes from a cubic to a rhombohedral at 0.5:1Co:Ti. FTIR reveals twin peaks for rhombohedral phase at 540 and 658cm^{-1}.

4.3 CONCLUSIONS

Thin films and powders with different stiochiometry of cobalt titanium oxide have been prepared by using the sol-gel technique. The surfaces were all annealed at 400°C and 800°C under a temperature program in order to remove any organic residues. The crystalline nature of the powders was identified by X-ray diffraction. XRD shows that high Co concentration ranging from 1:1 to 0.7:1 form a cubic phase with Co_2TO_4 structure and low Co concentration ranging from 0.5:1 to 0.3:1 form a rhombohedral phase with $CoTiO_3$ structure. Thin films could not be detected because they could be amorphous. SEM has shown that the cobalt titanate film surfaces deposited on Si substrate are rough with cracks. For Ti substrate, it reveals that the surfaces were smooth, uniform and crack-free. This is dependent to the film-substrate interaction. AFM confirms that the 1:1 and 0.5:1 Co:Ti have two phases. The 0.5:1 Co:Ti has a triangle-like particles which is organized in a regular manner and the 0.7:1 has a rod-like particles. The 1:1 Co:Ti has a large particle size of 0.6nm to 1μm while the 0.5:1 Co:Ti has small particle size of 400nm. AFM and FTIR agree with XRD results showing these cobalt titanates have different phases. RBS suggested that the 1:1 and 0.5:1Co:Ti have $Co_{1.39}TiO_{2.29}$ and $CoTiO_{4.2}$ structures respectively with 13nm and 16nm thickness.

CHAPTER 5

GENERAL CONCLUSIONS AND RECOMMEDATION FOR FUTURE WORK

5.1 GENERAL CONCLUSIONS

Thin films and powders with different stiochiometry (nickel titanium oxide and cobalt titanium oxide) were prepared by using sol-gel techniques. The materials were all annealed at 400°C and 800°C under a temperature program in order to remove any organic residues. The crystalline nature of the powders was identified by X-ray diffraction. XRD shows that all the ratios of Ni to Ti (0.3,0.5,0.7,0.9 and 1:1Ni:Ti) form $NiTiO_3$ powder. The best route for $NiTiO_3$ preparation is with a low concentration of Ni with respect to Ti, namely 0.3:1. For cobalt titanate, it was found that high Co concentration ranging from 1:1 with Ti to 0.7:1 form a cubic phase with the Co_2TO_4 structure. Low Co concentrations ranging from 0.5:1 to 0.3:1 with respect to Ti form a rhombohedral phase with $CoTiO_3$ structure. Thin films of nickel and cobalt titanates were found to be amorphous.

SEM has showed that the $NiTiO_3$ film surface deposited on a silicon substrate is smooth, uniform and crack-free. It also showed that the cobalt titanate film surfaces deposited on the Si substrate were rough with cracks. For Ti substrates, it revealed that the surfaces were smooth, uniform and crack-free. This is dependent on the film-substrate interaction. AFM has shown that as the ratio of Ni:Ti is reduced, the roughness of the thin film increases. It was found that the 0.7:1 $NiTiO_3$ has a moother surface than the films prepared with lower ratios of Ni:Ti. SEM, XRD and RBS suggested that the 0.3:1 and 0.5:1Ni:Ti films have the same $NiTiO_3$ structure at a film thickness of 10nm and 11nm, respectively. AFM confirmed that the 1:1 and 0.5:1

Co:Ti had two phases. The 0.5:1 Co:Ti has triangle-like particles which are organized in a regular manner and the 0.7:1 has a rod-like particles. The 1:1 Co:Ti has a large particle size of 0.6nm to 1μm, while the 0.5:1 Co:Ti has small particle sizes of 400nm. AFM results are in agreement with XRD results, showing these cobalt titanates have different phases. RBS suggested that the 1:1 and 0.5:1 Co:Ti has $Co_{1.39}TiO_{2.29}$ and $CoTiO_{4.2}$ structures respectively with 13nm and 16nm thickness. These metal titanate film electrodes were successfully prepared and characterized for evaluating interfacial oxidative processes at liquid/solid surfaces.

5.2 FUTURE WORK AND TRENDS

Perovskites of metal oxides are of great interest due to their wide range of physical properties, which include: ferro electrics, pyro electric and dielectric behaviour, that vary with the average valency of the transition metal used. These metal oxide electrodes ($NiTiO_3$ and $CoTiO_3$) could be evaluated for interfacial oxidative processes at liquid surfaces and also be used to study the influence of corrosive gases on the structure of ABO_3 films.

CHAPTER 6

REFERENCES

1. P. A. Cox; Transition metal oxides, Clarendon Press, Oxford, (1995).

2. Greenwood, N. N and Earushaw, A; Chemistry of elements, Pergamon, Oxford (1984).

3. Goodenough, J. B; Prog. Solid State Chem, 5, 145, (1971).

4. Seung-Hee Nam and Ho-Gi Kim; J. Appl. Phys., 72(7), 2895-99, (1992).

5. Hiratani, M; Tarutani, Y; Fukazawa, T; Okamoto, M and Takagi, K; Thin Solid Films, 227, 100-104, (1993).

6. Livage, J; Encyclopedia of Inorganic Chemistry,Ed by King; R. B. Chichester, John Wiley and Sons, pp3836, (1994).

7. Kamalasanan, M.N; Kumar, N.D and Chandra, S; J. Appl. Phys.,74(1), (1993).

8. FrÖhlich, K; Machajdik, D; Rosova, A; Vavra, I; Weiss, F; Bochu, B; Senateur, J.P; Thin Solid Films, 260, 187-191, (1995).

9. Beudale, P; Venigalla, S; Ambrose, J.R; Verink, E.D; Jr. and Adair, J.H; J. Am. Ceram. Soc., 76(10), 2619-27, (1993).

10. Mallick, K.K; Hartridge, A; Woodhead, J.L; and Bhattachanga, A.K; J. Mat. Sc., 31, 267-271, (1996).

11. Fujishima, A and Honda, K; Nature, 238, 37-38 (1992).

12. Galasso, F.S; Structure, Properties and Preparation of Perovskite-type compounds; Pergamon Press; London, (1969).

13. Wells, A. F; In Structural Inorganic Chemistry, 5th ed; Oxford Science Publications, Clarendon Press; Oxford, (1986).

14. IEEE Standard Definitions of Primary Ferroelectric Terms; Std. 180-1986, (1986), New York.

15. Nye, J.F; Physical Properties of Crystals; Their Representation by Tensors and Matrices; Oxford Science Publications; Oxford, (1985).

1.6. Newnham, R.E; In Structure- Property Relations; Springer-verlag, New York, (1975).

17. Jona, F and Shirane, G; Ferroelectric Crystals; Macmillan, New York, (1962).

18. Azaroff, L. V. Introduction to Solids; Mc Graw-Hill, NewYork, (1960).

19. Brooke, R.J; Cahn, R.W and Bever, M.B; Concise Encyclopedia of Advanced Ceramic Materials; Pergamon Press: Cambridge, (1991).

20. Jaffe, B; Cooke, W.R and Jaffe, H.L.C; Piezoelectric Ceramics; Academic Press: New York, (1971).

21. Mott, N.F; J. Non-cryst. Solid, 1, 1, (1968).

22. Austin, I.G and Mott, N.F; Adv. Phys., 18, 41, (1969).

23. Chung, C.H; Mackenzie, J.D and Murawski L; Rev. Chemie Minerale., 16, 308, (1979).

24. England, W.A; Cross, M.G; Hamnett, A; Wiseman, P.J and Goodenough, J.B; Solid State Ionics, 1, 231, (1980).

25. Ruvarac, A; Inorganic ion exchange materials, A. Clearfield Ed, C.R.C Press,

Boca Roton, pp141, (1982).

26. Yamanaka, K; Oakamoto, H; Kidon, H and Kudo, T; J. Appl. Phys., 25, 1420, (1986).
27. Yoshino, T; Baba, N and Konda, Y; J. Appl. Phys., 26, 782, (1987).
28. Henglein, A; Pure and Appl. Chem., 56, 1215, (1984).
29. Turner, C.W; Ceramic Bulletin, 70, 1487-1490, (1991).
30. Wilson, G and Pateel; A. Mater. Sci. Technol, 9, 937-944, (1993).
31. Dislich, H; J. Non-Cryst. Solid., 73, 599-612, (1985).
32. Roy, R; Science, 238, 1664-1669, (1987).
33. Segal, D; Chemistry in Britain., 151-156, (1989).
34. Xu, Y and Mackenzie, J.D; Intergrated Ferroelectrics, 1, 17-42, (1992).
35. Suyama, Y and Nagasawa, M; J. Am. Ceramic. Soc., 77, 603-605, (1994).
36. Woei-kwo Kuo and Yong-chein Ling; J. Mater. Sc, 29, 5625-5630, (1994).
37. Chaput, F; Boilot, J.P and Beauger; A. J. Am. Ceram. Soc., 73, 942-994, (1990).
38. Lemoine, C; Gilbert, B; Michaux, B; Pirard, J.P and Lecloux, A.J; J. Non-Cryst. Solids., 175, 1-13, (1994).
39. Respringer, J.L; Poix, P and Bernier, J.C; J. Non-Cryst. Solids, 82, 286-292, (1986).
40. Rodriguez-Reinoso, F; Roquerol, J; Sing, K.S.W and Unger, K.K; (editors), Characterization of Porous Solid II, Elsevier, Amsterdam, (1991).
41. Terenin, A; Adv. Catal, 30, 227, (1981).
42. Bhatia, S; Beltramini, J and Do, D.D; Catal. Today, 7, 309, (1990).

43. Flewit, P.E.J and Wild, R.K; Physical Methods for Materials Characterisation, I.O.P. Publishing Ltd (1994).

44. Postek, M.T; Howard, K.S; Johnson, A.H and Mc Michael, K.L; Scanning Electron Microscopy, Student Handbook.

45. Grundy, P. J and Jones, G. A; Eletron Microscopy in the study of materials, Edward Arnold Limited Publishers, (1976).

46. Low, M. J. D; Mark, H and Goodsel, A. J., Molecular spectroscopy, Institute of Petroleum, London, (1971).

47. Hair, M. L; Infrared Spectroscopy in Surface Chemistry, Dekker, New York, (1966).

48. Willard, H. H; Merrit, L. L; Dean, J. A and Settle, F. A; Instrumental Methods of Analysis., 7th ed., Wadsworth publishing Co., California, (1988).

49. Last, J. T; Physical Review, 105(6), 1740 (1957).

50. Moreno, G;Tavizon, L; Vicente; Material Research Society Process, 435, 315–320, (1996).

51. Blanplain, B; Revesz, P; Doolittle, L.R; Purser, K.H and Mayer, J.W; Nuclear Instruments and Methods in physics Research B34 459-464, (1988).

52. Guenther, K.H; McCandless, J.A and Orazio, F.D; Jr., Correlation of light scattering measurements and visual ranking if optical surfaces, Appl. Opt. 32, (1993).

53 Scherer, W; "Aging and Drying of Gel," J. Non-cryst. Solids, 100, 88,

(1988).

54. Tian, H; Luo, W; Pu, X; Qiu, P; He, X and Ding, A; Thermochimica Acta, 360, 57-62, (2000).

55. Guenther, K.H; Wierer, P.G and Bennett, J.M. Surface roughness measurements of low scatter mirrors and roughnessstandards, Appl.Opt. 23, 3820-3833, (1984).

7.0 ANNEX

7.1 PHOTOELECTROCHEMICAL INVESTIGATION

The excitation light source was a 900W Xe lamp operating at 300W. This set up was utilised to test the photoelectrochemical behaviour of the catalyst (metal oxides) for the target molecules (metal cyanide complexes). The experimental set up of the cell was as follows: thin film electrode (working electrode), Pt electrode (auxiliary electrode), target molecules (electrolyte). Voltage readings ($E_{reading} = E_{working} + E_{auxiliary}$) were obtained for all runs, each run lasted an hour. The cell was initially left in the dark for 10 minutes, illuminated for 25 minutes, in the dark for a further 10 minutes, illuminated for further 10 minutes and finally left in the dark for a further 5 minutes. The target molecule was exposed to the different stiochemistry of the following electrodes: TiO_2, $NiTiO_3$ and $CoTiO_3$.

A potential of -0.5V to 0.5V from BAS CV-27 was applied across the working electrode (TiO_2, $NiTiO_3$ and $CoTiO_3$ thin film electrodes) and the reference electrode (Ag\AgCl) with photovoltage readings recorded at intervals (every 0.1V) of applied potential. Photovoltage readings were recorded on a multimeter (Fluke series 711) utilising the thin film electrodes as working electrodes and platinum electrode as the counter electrode. KCN (50ppm in 0.01M NaOH) was used as the electrolysing solution. Graphs of applied potential versus photovoltage were plotted to determine the flat-band potentials of the metal oxides thin films.

Photoelectrochemical profiles of various metal cyanides were studied utilising the metal titanate thin surfaces as the photoelectodes viz.

1.Titanium oxide

2. Nickel titanium oxide

3. Cobalt titanium oxide

Figure 7.1: Voltage Vs time profile for $CoTiO_{18.6}$ in the presence of $K_3Fe(CN)_6$

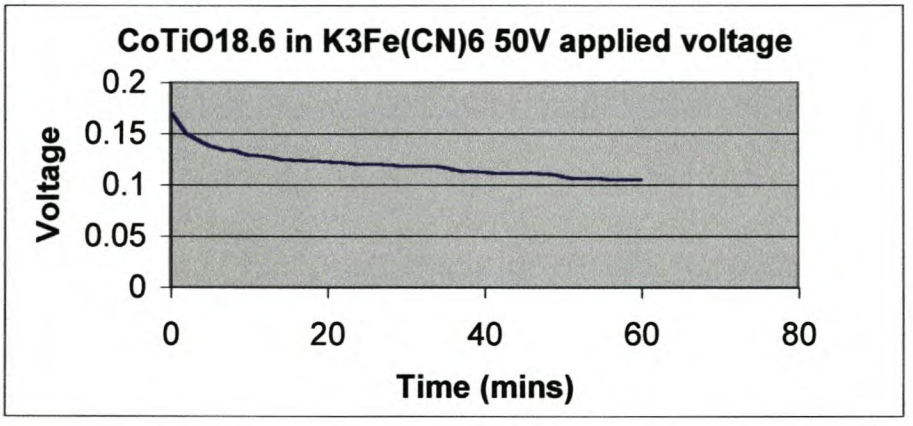

Figure 7.1 above shows the photo-voltage profiles of a metal cyanide when the $CoTiO_{18.6}$ thin film electrode was used as photoelectrode. For the first 10 minutes the redox potentials of the photoelectrode and the electrolytes (metal cyanides) were allowed to reach equilibrium. On irradiation (10-35 min), we expected an increase in photo-voltage reponses for the metal cyanides. Figure 7.1 shows that there was no photoelectrochemical process happening. Even for TiO_2 thin film electrode as photoelectrode, which has published photoelectrochemical data's, show no photoelectrochemical processes. This is because the TiO_2 electrode was prepared by a sol-gel process. The photoelectrochemical results of cobalt and nickel titanates were negative. These metal oxides (TiO_2, $NiTiO_3$ and $CoTiO_3$) were photochemical

inactive. At this stage no quantitable explaination is offered for the lack of photochemical activity.